PERGAMON

International Journal of Solids and Structures 38 (2001) 9077–9109

INTERNATIONAL JOURNAL OF SOLIDS and STRUCTURES

www.elsevier.com/locate/ijsolstr

Analysis of singular stress fields at junctions of multiple dissimilar materials under mechanical and thermal loading

A. Barut, I. Guven, E. Madenci *

Department of Aerospace and Mechanical Engineering, University of Arizona, P.O. Box 210119, Tucson, AZ 85721, USA

Received 28 November 2000; in revised form 17 August 2001

Abstract

Traditional finite element analyses of the stress state in regions with dissimilar materials are incapable of correctly resolving the stress state because of the unbounded nature of the stresses. A finite element technique utilizing a coupled global (special) element with traditional elements is presented. The global element includes the singular behavior at the junction of dissimilar materials with or without traction-free surfaces. A hybrid global (special) element is developed utilizing the exact solution for the stress and displacement fields based on the eigenfunction expansion method under mechanical and thermal loading. The global element for arbitrary geometrical and material configurations, not limited to a few dissimilar material sectors, is interfaced with traditional local (conventional) elements while satisfying the inter-element continuity. The coupling between the hybrid global element and conventional finite elements is implemented into ANSYS, a commercially available finite element program. Also, the global element is integrated into the ANSYS graphical user interface for pre- and post-processing. © 2001 Elsevier Science Ltd. All rights reserved.

Keywords: Finite region; Dissimilar material junctions; Thermal and mechanical loading

1. Introduction

Adhesive bonding is a primary means for constructing components of layered material systems, such as a microelectronic package. The primary components of these packages are the die, the die-attach (adhesive), and the substrate. The packages are usually subjected to temperature excursions during manufacturing and testing. These excursions, combined with the different thermal expansion coefficients of the package components, result in residual thermal stresses. A layered system of materials responds differently, depending on the combined interaction of thermal and mechanical loads and the geometry of the dissimilar material junctions. These junctions are formed by sectors (wedges) of different materials bonded together. High stress gradients are known to exist in the vicinity of the junction due to mismatch in thermal

* Corresponding author. Tel.: +1-520-621-6113; fax: +1-520-621-8191.
E-mail address: madenci@email.arizona.edu (E. Madenci).

0020-7683/01/$ - see front matter
PII: S0020-7683(01)00206-2

expansion coefficients and in elastic moduli. As reported by Williams (1952), the stress state near the junction often has a singular behavior and the nature of the singularity is a function of the junction geometry and elastic constants of the materials. Delamination and cracking failures usually initiate at these junctions, influencing the reliability of the packages. Hence, it is essential to understand the effect of geometry and material parameters on the singular behavior of the stress field near the junction of dissimilar materials under combined mechanical and thermal loadings.

Previous analytical studies by Bogy (1968), Hein and Erdogan (1971), and Theocaris (1974) were concerned with asymptotic solutions with the leading order term only; thus, the stress field was accurate at a distance very close to the junction point. Munz and Yang (1992, 1993) and Munz et al. (1993) extended the asymptotic solution method to investigate the stress field due to a change in uniform temperature near the free edge of a junction of dissimilar materials. Inoue and Koguchi (1997) discussed the characteristics of the stress intensity factors in a composite wedge of dissimilar materials under thermal loading and identified conditions for which the stress intensity factors disappear. Recently, Gadi et al. (2000) investigated the thermally induced logarithmic stress singularities in a composite wedge of dissimilar materials and provided the solution form in the presence of double and triple roots of the characteristic equations leading to non-separable eigenfunctions. The asymptotic stress field at distances slightly away from the junction point suffers from accuracy, as reported by Qian and Akisanya (1999). Furthermore, the asymptotic solutions only provide information on the strength of the singular behavior, not on the intensity of the singularity essential for predicting failure initiation. However, the asymptotic solutions provide accurate values for the stress intensity factors if the dissimilar material junction coincides with a crack tip. Also, the asymptotic solutions served as interpolation functions in constructing special elements as part of the traditional finite element analysis in order to capture the exact singular behavior of the stress field.

Concerning a crack lying either along the interface or perpendicular to the interface, Lin and Mar (1976) developed a hybrid crack element for a bi-material interface. The assumed stress and displacement fields for the hybrid element were derived based on the complex potential technique. In modeling a free edge with a bi-material interface, Chen (1985) developed an element with appropriate interpolation functions built in to account for the singularity at the free edge of a bi-material interface crack subjected to mechanical loading only. Similar to Chen's work, Gadi et al. (1995) and Pageau and Biggers (1996, 1997) developed enriched finite elements that account for the singular behavior at the junction of dissimilar materials. Extending the work by Mote (1971) and Bradford et al. (1984), Madenci et al. (1998) developed a global (special) element based on the asymptotic solution for dissimilar material junctions and coupled it with conventional elements.

In all of these coupled special elements with built-in leading-order singularity and conventional elements, the results are dependent on the special element's size. In order to enhance the accuracy of the results, these enriched elements usually employ transition (overlap) elements, thus introducing another degree of uncertainty as to the extent of the zone for the transition elements. Also, inter-element compatibility between the special and conventional elements is not satisfied, except for the special hybrid element by Lin and Mar (1976). Thus, monotonic convergence of the results is not guaranteed. Also, these analyses are limited to junctions of a few dissimilar materials.

In an effort to characterize the singularities at free edges with or without a crack, Munz and Yang (1992) developed fifth-order polynomial expressions in terms of the leading-order term for the stress intensity factors by combining the asymptotic solution with finite element analysis in conjunction with curve-fitting techniques. Later, Akisanya and Fleck (1997) developed a method that utilizes a traditional finite element combined with Betti's reciprocal theorem involving a path-independent contour integral. This study involved the evaluation of the stress intensity factor for a free-edge interface crack, the intensity of singularity of a junction of dissimilar materials with a traction-free edge without a crack, and the strength of singularity using the asymptotic solution. As an extension of this approach, Qian and Akisanya (1999) showed that the asymptotic solution with a leading-order term is not sufficient to capture the accurate behavior of

the singular stress field near the junction. Solutions obtained by this method are also dependent on the finite element mesh density influencing the numerical evaluation of the path-independent integral.

In order to eliminate the aforementioned shortcomings while addressing either an open or a closed junction of multiple dissimilar materials as shown in Fig. 1, a hybrid global (special) element is developed utilizing the exact solution for the stress and displacement fields based on the eigenfunction expansion method under mechanical and thermal loading. The global element for arbitrary geometrical and material configurations, not limited to a few dissimilar material sectors, is interfaced with traditional local (conventional) elements while satisfying the inter-element continuity. The coupling between the hybrid global element and conventional finite elements is implemented into ANSYS, a commercially available finite element program. Also, the global element is integrated into the ANSYS graphical user interface for pre- and post-processing.

The validity of this approach is established through existing asymptotic solutions and conventional detailed finite element analysis. The first validation problem involves a plate of two dissimilar materials under either uniform tension or uniform temperature change. The second validation problem involves an interface crack in a bi-material plate under uniform tension. The third validation problem concerns the

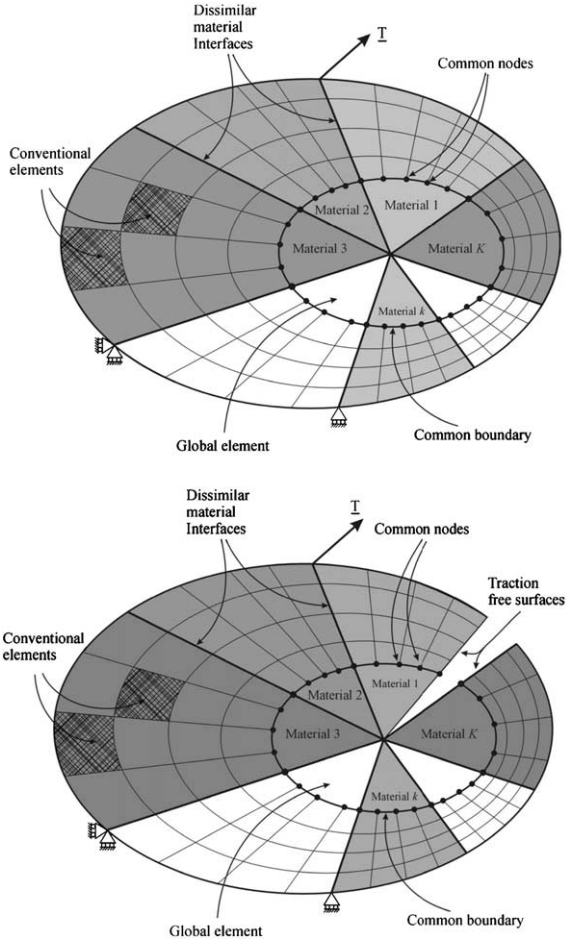

Fig. 1. Conventional elements coupled with a global element for a closed and open junction.

stress intensity factors at a crack tip perpendicular to the interface of a bi-material strip under uniform strain. In the presence of a crack, the stress intensity factors and the J-integral values are calculated, and their dependence on the global element size and the number of eigenvalues retained in the analysis is presented. The stress intensity factors are also calculated for a crack situated between two semi-circular inclusions embedded in a different material under uniform temperature.

2. Solution method

As illustrated in Fig. 1, a domain composed of multiple dissimilar material sectors can be partitioned into inner and outer regions. In the inner region of either a closed or open junction, the presence of a singular stress field near the junction arising from the material and geometric discontinuities requires an exact solution of the governing equations. The solution to the outer region in which a singular stress field does exist can be constructed by employing the finite element method with conventional elements. Therefore, an accurate solution to the entire domain requires coupling of the exact solution in the inner region with that of the approximate solution through the finite element method in the outer region. The coupling can be achieved by developing a global element whose interpolation functions satisfy the governing equations exactly near the junction while enforcing the inter-element displacement continuity along the common boundary and the nodes between the global and conventional elements.

Each sector of the domain forming either a closed or open junction represents an elastic, homogeneous, and isotropic material with Young's modulus, E_k, Poisson's ratio, ν_k, and a thermal expansion coefficient, κ_k. The interface between the $(k-1)$th and the kth material sectors is defined by the angle θ_k and is denoted by $I^{(k-1,k)}$. Perfect bonding with zero thickness is assumed along these interfaces. As shown in Fig. 2, the interface angles are measured in the counterclockwise direction from the reference Cartesian coordinate

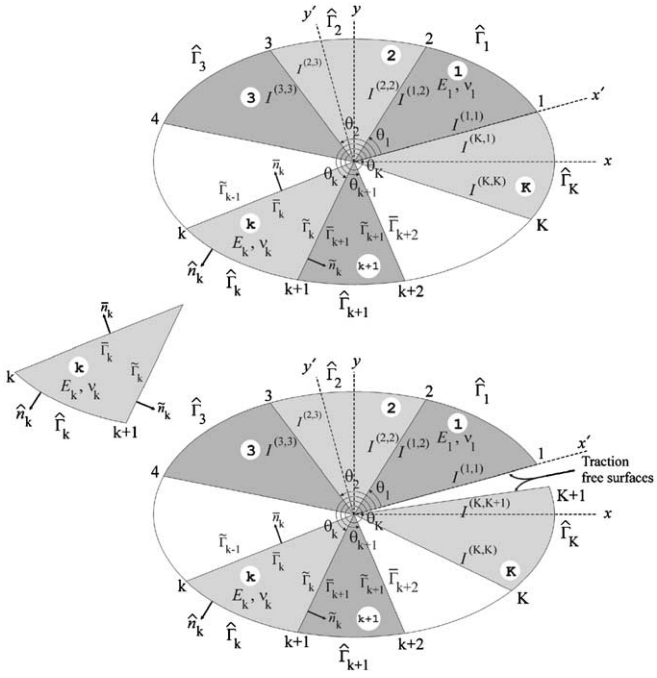

Fig. 2. Description of the global element geometry and numbering of the material sections and the interfaces.

system (x', y') whose horizontal axis is aligned with the first radial boundary of the first material sector. Its origin and the origin of a global Cartesian coordinate system (x, y) coincide with the junction.

As shown in Fig. 2, the kth segment of the inner region (global element) boundary associated with the kth material sector is denoted by $\hat{\Gamma}_k$, and its unit normal to the boundary is $\hat{\mathbf{n}}^{(k)}$. Along the interfaces labeled as $I^{(k-1,k)}$ and $I^{(k,k+1)}$, the radial boundaries of the kth sector and their unit normal vectors are denoted by $\overline{\Gamma}_k$, $\bar{\mathbf{n}}^{(k)}$ and $\widetilde{\Gamma}_k$, $\tilde{\mathbf{n}}^{(k)}$, respectively. The distinction in notation for the boundaries and their corresponding unit normal vectors of each sector of the region facilitates the simplification of total potential energy expression for the global element. It is worth mentioning that the solution method is developed under plane stress assumptions. Therefore, the material constants must be adjusted according to $E'_k = E_k/(1 - \nu_k^2)$, $\nu'_k = \nu_k/(1 - \nu_k)$, and $\kappa'_k = \kappa_k(1 + \nu_k)$ when considering plane strain conditions.

2.1. Interpolation functions for the global element

As suggested by Williams (1952) and later extended by Munz et al. (1993), for combined mechanical and uniform thermal loading, the stress and displacement components in the kth material sector are represented by

$$\sigma_{\alpha\beta}^{(k)}(r,\theta) = \sum_{n=0}^{\infty} r^{\lambda_n} F_{\alpha\beta}^{(k)}(\theta;\lambda_n) + f_{\alpha\beta}^{(k)}(\theta) \tag{1}$$

and

$$u_{\alpha}^{(k)}(r,\theta) = \sum_{n=0}^{\infty} r^{\lambda_n+1} G_{\alpha}^{(k)}(\theta;\lambda_n) + r\left[g_{\alpha}^{(k)}(\theta) + \kappa_k T_0 \delta_{r\alpha}\right] + r\ln r h_{\alpha}^{(k)}(\theta) \tag{2}$$

with $\alpha, \beta = r, \theta$ $(k = 1, 2, \ldots, K)$, $\lambda_0 = 0$, and $\lambda_n \neq 0$ for $n = 1, 2, \ldots, N$. The origin of the polar coordinate system (r, θ) coincides with the junction of the vertices. The unknown parameter, λ_n is a global variable and that it is valid for each sector of the inner region. It depends on the material properties, the geometric configurations and the number of material sectors. The uniform temperature change is denoted by T_0, and the symbol $\delta_{\alpha\beta}$ represents the Kronecker delta. Under plane stress conditions, the non-dimensional functions $F_{\alpha\beta}^{(k)}(\theta;\lambda_n)$, $G_{\alpha}^{(k)}(\theta;\lambda_n)$, $f_{\alpha\beta}^{(k)}(\theta)$, $g_{\alpha}^{(k)}(\theta)$ and $h_{\alpha}^{(k)}(\theta)$ satisfying the equilibrium and compatibility equations are expressed explicitly in Appendix A. The non-singular stress and displacement terms arising from thermal loading are captured through $f_{\alpha\beta}^{(k)}(\theta)$, $g_{\alpha}^{(k)}(\theta)$ and $h_{\alpha}^{(k)}(\theta)$. This representation of the displacement field is identical to that of suggested by Gadi et al. (2000) for $\lambda_0 = 0$. As explained later in this section, the roots of multiplicity for $n \geqslant 0$ are identified and the solution is constructed by redefining the solution vector as the linear combination of independent eigenvectors.

Prior to enforcing the continuity equations and boundary conditions, a combination of these functions is recast as

$$\mathbf{p}_n^{(k)}(\theta;\lambda_n) = \mathbf{P}_n^{(k)}(\theta;\lambda_n)\mathbf{q}_n^{(k)}; \quad n = 0, 1, \ldots, N \tag{3}$$

$$\mathbf{p}_c^{(k)}(\theta) = \mathbf{P}_c^{(k)}(\theta)\mathbf{q}_c^{(k)} \tag{4}$$

and

$$\mathbf{t}_n^{(k)}(\theta;\lambda_n) = \mathbf{T}_n^{(k)}(\theta;\lambda_n)\mathbf{q}_n^{(k)}; \quad n = 0, 1, \ldots, N \tag{5}$$

$$\mathbf{t}_c^{(k)}(\theta) = \mathbf{T}_c^{(k)}(\theta)\mathbf{q}_c^{(k)} \tag{6}$$

in which the vectors $\mathbf{p}_c^{(k)}$, $\mathbf{p}_n^{(k)}$, $\mathbf{t}_c^{(k)}$, $\mathbf{t}_n^{(k)}$, $\mathbf{q}_c^{(k)}$, and $\mathbf{q}_n^{(k)}$ are defined by

$$\mathbf{p}_c^{(k)^T} = \left\{ f_{\theta\theta}^{(k)}(\theta), f_{r\theta}^{(k)}(\theta), g_r^{(k)}(\theta), g_\theta^{(k)}(\theta), h_\theta^{(k)}(\theta) \right\} \tag{7}$$

$$\mathbf{p}_n^{(k)^T} = \left\{ F_{\theta\theta}^{(k)}(\theta;\lambda_n), F_{r\theta}^{(k)}(\theta;\lambda_n), G_r^{(k)}(\theta;\lambda_n), G_\theta^{(k)}(\theta;\lambda_n) \right\} \tag{8}$$

$$\mathbf{t}_c^{(k)^T} = \left\{ f_{\theta\theta}^{(k)}(\theta), f_{r\theta}^{(k)}(\theta) \right\} \tag{9}$$

$$\mathbf{t}_n^{(k)^T} = \left\{ F_{\theta\theta}^{(k)}(\theta;\lambda_n), F_{r\theta}^{(k)}(\theta;\lambda_n) \right\} \tag{10}$$

$$\mathbf{q}_c^{(k)^T} = \left\{ A_c^{(k)}, B_c^{(k)}, C_c^{(k)}, D_c^{(k)}, E_c^{(k)} \right\} \tag{11}$$

$$\mathbf{q}_n^{(k)^T} = \left\{ A_n^{(k)}, B_n^{(k)}, C_n^{(k)}, D_n^{(k)} \right\} \tag{12}$$

The explicit form of matrices $\mathbf{P}_c^{(k)}$, $\mathbf{P}_n^{(k)}$, $\mathbf{T}_c^{(k)}$, and $\mathbf{T}_n^{(k)}$ are given in Appendix A.

In the case of an open junction, the traction-free boundary conditions and the continuity conditions between the adjacent sectors are given by

$$\mathbf{t}_c^{(1)}(0) = \mathbf{t}_c^{(K)}(\theta_K) = 0 \tag{13}$$

$$\mathbf{t}_n^{(1)}(0;\lambda_n) = \mathbf{t}_n^{(K)}(\theta_K;\lambda_n) = 0 \tag{14}$$

$$\mathbf{p}_c^{(k)}(\theta_k) - \mathbf{p}_c^{(k+1)}(\theta_k) = \mathbf{r}_c^{(k)} - \mathbf{r}_c^{(k+1)} \tag{15}$$

$$\mathbf{p}_n^{(k)}(\theta_k;\lambda_n) - \mathbf{p}_n^{(k+1)}(\theta_k;\lambda_n) = \mathbf{0} \tag{16}$$

with $k = 1, \ldots, K-1$ and $n = 0, \ldots, N$.

In the case of a closed junction, the continuity conditions between the adjacent sectors are given by

$$\mathbf{p}_c^{(1)}(0) - \mathbf{p}_c^{(K)}(2\pi) = \mathbf{r}_c^{(1)} - \mathbf{r}_c^{(K)} \tag{17}$$

$$\mathbf{p}_n^{(1)}(0;\lambda_n) - \mathbf{p}_n^{(K)}(2\pi;\lambda_n) = \mathbf{0} \tag{18}$$

$$\mathbf{p}_c^{(k)}(\theta_k) - \mathbf{p}_c^{(k+1)}(\theta_k) = \mathbf{r}_c^{(k)} - \mathbf{r}_c^{(k+1)} \tag{19}$$

$$\mathbf{p}_n^{(k)}(\theta_k;\lambda_n) - \mathbf{p}_n^{(k+1)}(\theta_k;\lambda_n) = \mathbf{0} \tag{20}$$

with $k = 1, \ldots, K-1$ and $n = 0, \ldots, N$. The vector $\mathbf{r}_c^{(k)}$ is defined as

$$\mathbf{r}_c^{(k)^T} = \{0, 0, -\kappa_k T_0, 0, 0\} \tag{21}$$

Along with the boundary conditions and continuity of displacement and traction components, it is necessary to suppress the rigid-body rotation of any one of the material sectors. Without loss of generality, the rigid-body rotation mode arising from the complementary solution is prevented by requiring that

$$\frac{\nu_k - 3}{4E_k} C_c^{(1)} + E_c^{(1)} = 0 \quad \text{or} \quad \mathbf{C}_R^T \mathbf{q}_c^{(1)} = 0 \tag{22}$$

where $\mathbf{C}_R^T = \{0, 0, \nu_1 - 3/E_1, 0, 1\}$. This constraint eliminates the constant terms arising in the expression given explicitly in Appendix A.

Enforcing these conditions associated with either a closed or an open junction of K dissimilar material sectors leads to a non-homogeneous and a homogeneous system of equations in the form

$$\mathbf{S}_j\mathbf{q}_c = \mathbf{r}_j \quad \text{and} \quad \mathbf{Q}_j(\lambda_n)\mathbf{q}_n = \mathbf{0} \tag{23}$$

with $j = \mathrm{C}, \mathrm{O}$; the subscript j indicates the type of junction. The subscripts C and O refer to the closed and open junction, respectively. The vectors of unknown coefficients $\mathbf{q}_c$ and $\mathbf{q}_n$ are defined by

$$\mathbf{q}_c^T = \left\{\mathbf{q}_c^{(1)^T}, \mathbf{q}_c^{(2)^T}, \mathbf{q}_c^{(3)^T}, \ldots, \mathbf{q}_c^{(K-1)^T}, \mathbf{q}_c^{(K)^T}\right\} \tag{24}$$

and

$$\mathbf{q}_n^T = \left\{\mathbf{q}_n^{(1)^T}, \mathbf{q}_n^{(2)^T}, \mathbf{q}_n^{(3)^T}, \ldots, \mathbf{q}_n^{(K-1)^T}, \mathbf{q}_n^{(K)^T}\right\} \tag{25}$$

The known vectors, $\mathbf{r}_j$, the coefficient matrices, $\mathbf{S}_j$ and $\mathbf{Q}_j$ with $j = \mathrm{C}, \mathrm{O}$, are given explicitly in Appendix A.

A non-trivial solution to the homogeneous system exists for values of λ_n that cause the determinant of the coefficient matrix $\mathbf{Q}_j(\lambda_n)$ to vanish. They may be complex, depending on the properties of the material sectors. These particular values of λ_n are the roots of the characteristic equation

$$\left|\mathbf{Q}_j(\lambda_n)\right| = 0 \quad \text{with } n = 0, 1, \ldots, N \tag{26}$$

The roots may be repeated or distinct. However, the numerical solution of the characteristic equation does not readily reveal the multiplicity of each root, λ_n. Therefore, an auxiliary homogeneous system of equations is constructed in the form of a complex eigenvalue problem

$$\left[\mathbf{Q}_j(\lambda_n) - \Lambda\mathbf{I}\right]\mathbf{q}_n = \mathbf{0} \tag{27}$$

in order to determine the multiplicity of each root. The unknown parameter Λ represents the eigenvalue, and $\mathbf{I}$ is the identity matrix. Considering the root λ_n, the eigenvector(s) arising from zero eigenvalue(s), $\Lambda = 0$, establishes the multiplicity of the root λ_n and the solution vector for

$$\mathbf{Q}_j(\lambda_n)\mathbf{q}_n = \mathbf{0} \tag{28}$$

Therefore, the solution vector, $\mathbf{q}_n$, associated with the root, λ_n, can be constructed as a linear combination of the independent eigenvectors, $\bar{\mathbf{q}}_{nr}$, corresponding to $\Lambda_r = 0$, with $r = 1, \ldots, R_n$, in the form

$$\mathbf{q}_n = \sum_{r=1}^{R_n} \alpha_{nr}\bar{\mathbf{q}}_{nr} \tag{29}$$

in which R_n denotes the multiplicity of the root, λ_n, and α_{nr} represents the unknown constants.

In accordance with the definition of $\mathbf{q}_n$, the known eigenvector $\bar{\mathbf{q}}_{nr}$ is defined as

$$\bar{\mathbf{q}}_{nr}^T = \left\{\bar{\mathbf{q}}_{nr}^{(1)^T}, \bar{\mathbf{q}}_{nr}^{(2)^T}, \bar{\mathbf{q}}_{nr}^{(3)^T}, \ldots, \bar{\mathbf{q}}_{nr}^{(K-1)^T}, \bar{\mathbf{q}}_{nr}^{(K)^T}\right\} \tag{30}$$

The homogeneous solution given in Eq. (29) includes a rigid-body rotation mode for $n = 0$. Therefore, the rigid-body modes appearing in the generalized coordinates are suppressed by imposing the condition of no-rigid-body rotation in the form

$$\sum_{r=1}^{R_n} \alpha_{0r}\bar{b}_{0r}^{(1)} = 0 \quad \text{or} \quad \alpha_{01} = -\sum_{r=2}^{R_n} \frac{\bar{b}_{0r}^{(1)}}{\bar{b}_{01}^{(1)}}\alpha_{0r} = 0 \tag{31}$$

in which $\bar{b}_{0r}^{(1)}$ are the second elements of the eigenvectors, $\bar{\mathbf{q}}_{0r}$. Invoking the expression for α_{01} directly into the Eq. (29) permits

$$\mathbf{q}_n = \sum_{r=1+\delta_{n0}}^{R_n} \alpha_{nr}\hat{\mathbf{q}}_{nr} \tag{32}$$

in which

$$\hat{\mathbf{q}}_{nr} = \begin{cases} \bar{\mathbf{q}}_{0r} - \frac{\bar{b}_{0r}^{(1)}}{\bar{b}_{01}^{(1)}}\bar{\mathbf{q}}_{01}; & (r = 2,\ldots,R_n) \text{ and } n = 0 \\ \bar{\mathbf{q}}_{nr}; & (r = 1,2,\ldots,R_n) \text{ and } n \neq 0 \end{cases}$$

and

$$\delta_{n0} = \begin{cases} 1; & n = 0 \\ 0; & n \neq 0 \end{cases}$$

Therefore, the solution vector defined in Eq. (32) is utilized in the vectorial representation of the stress and displacement fields.

The vectors of stress and displacement components are defined as

$$\boldsymbol{\sigma}_p^{(k)^T} = \left\{\sigma_{rr}^{(k)}, \sigma_{\theta\theta}^{(k)}, \sigma_{r\theta}^{(k)}\right\} \quad \text{and} \quad \mathbf{u}_p^{(k)^T} = \left\{u_r^{(k)}, u_\theta^{(k)}\right\} \tag{33}$$

and can be rewritten in the form

$$\boldsymbol{\sigma}_p^{(k)} = {}_\lambda{}^m\boldsymbol{\sigma}_p^{(k)} + {}_\lambda{}^t\boldsymbol{\sigma}_p^{(k)} + {}_c{}^t\boldsymbol{\sigma}_p^{(k)} \quad \text{and} \quad \mathbf{u}_p^{(k)} = {}_\lambda{}^m\mathbf{u}_p^{(k)} + {}_\lambda{}^t\mathbf{u}_p^{(k)} + {}_c{}^t\mathbf{u}_p^{(k)} \tag{34}$$

In these expressions for stress and displacement components, the terms ${}_\lambda{}^m\boldsymbol{\sigma}_p^{(k)}$, ${}_\lambda{}^m\mathbf{u}_p^{(k)}$ and ${}_\lambda{}^t\boldsymbol{\sigma}_p^{(k)}$, ${}_\lambda{}^t\mathbf{u}_p^{(k)}$ are associated with the homogeneous solutions of mechanical and thermal loadings, respectively. In the case of thermal loading, ${}_c{}^t\boldsymbol{\sigma}_p^{(k)}$ and ${}_c{}^t\mathbf{u}_p^{(k)}$ represent the known complementary solutions for non-singular stress and displacement fields. These vectors can be defined as

$$\left.\begin{aligned} {}_\lambda{}^m\boldsymbol{\sigma}_p^{(k)} &= \mathrm{Re}\left\{\sum_{n=0}^{N}\sum_{r=1+\delta_{n0}}^{R_n}\mathbf{F}_n^{(k)}(r,\theta;\lambda_n)\hat{\mathbf{q}}_{nr}^{(k)m}\alpha_{nr}\right\} \\ {}_\lambda{}^m\mathbf{u}_p^{(k)} &= \mathrm{Re}\left\{\sum_{n=0}^{N}\sum_{r=1+\delta_{n0}}^{R_n}\mathbf{G}_n^{(k)}(r,\theta;\lambda_n)\hat{\mathbf{q}}_{nr}^{(k)m}\alpha_{nr}\right\} \end{aligned}\right\} \tag{35}$$

$$\left.\begin{aligned} {}_\lambda{}^t\boldsymbol{\sigma}_p^{(k)} &= \mathrm{Re}\left\{\sum_{n=0}^{N}\sum_{r=1+\delta_{n0}}^{R_n}\mathbf{F}_n^{(k)}(r,\theta;\lambda_n)\hat{\mathbf{q}}_{nr}^{(k)t}\alpha_{nr}\right\} \\ {}_\lambda{}^t\mathbf{u}_p^{(k)} &= \mathrm{Re}\left\{\sum_{n=0}^{N}\sum_{r=1+\delta_{n0}}^{R_n}\mathbf{G}_n^{(k)}(r,\theta;\lambda_n)\hat{\mathbf{q}}_{nr}^{(k)t}\alpha_{nr}\right\} \end{aligned}\right\} \tag{36}$$

$${}_c{}^t\boldsymbol{\sigma}_p^{(k)} = \mathbf{F}_c^{(k)}(r,\theta)\mathbf{q}_c^{(k)}, \quad {}_c{}^t\mathbf{u}_p^{(k)} = \mathbf{G}_c^{(k)}(r,\theta)\mathbf{q}_c^{(k)} + r\kappa_k T_0\mathbf{e}_r \tag{37}$$

in which $\mathbf{e}_r^T = \{1,0\}$.

The vector $\hat{\mathbf{q}}_{nr}^{(k)}$ contains the known coefficients $\bar{A}_n^{(k)}$, $\bar{B}_n^{(k)}$, $\bar{C}_n^{(k)}$, and $\bar{D}_n^{(k)}$ in terms of α_{nr} corresponding to λ_n. The matrices $\mathbf{F}_n^{(k)}$, $\mathbf{G}_n^{(k)}$, $\mathbf{F}_c^{(k)}$, and $\mathbf{G}_c^{(k)}$ are defined as

$$\mathbf{F}_n^{(k)} = r^{\lambda_n}\begin{bmatrix} \frac{(2-\lambda_n)}{4}\cos\lambda_n\theta & \frac{(2-\lambda_n)}{4}\sin\lambda_n\theta & -\cos(2+\lambda_n)\theta & -\sin(2+\lambda_n)\theta \\ \frac{(2+\lambda_n)}{4}\cos\lambda_n\theta & \frac{(2+\lambda_n)}{4}\sin\lambda_n\theta & \cos(2+\lambda_n)\theta & \sin(2+\lambda_n)\theta \\ \frac{\lambda_n}{4}\sin\lambda_n\theta & -\frac{\lambda_n}{4}\cos\lambda_n\theta & \sin(2+\lambda_n)\theta & -\cos(2+\lambda_n)\theta \end{bmatrix} \tag{38}$$

and

$$\mathbf{G}_n^{(k)} = r^{\lambda_n+1}\begin{bmatrix} a_n^{(k)}\cos\lambda_n\theta & a_n^{(k)}\sin\lambda_n\theta & -b_n^{(k)}\cos(\lambda_n+2)\theta & -b_n^{(k)}\sin(\lambda_n+2)\theta \\ c_n^{(k)}\sin\lambda_n\theta & c_n^{(k)}\cos\lambda_n\theta & b_n^{(k)}\sin(\lambda_n+2)\theta & -b_n^{(k)}\cos(\lambda_n+2)\theta \end{bmatrix} \tag{39}$$

in which

$$a_n^{(k)} = \frac{(2-\lambda_n)-\nu_k(2+\lambda_n)}{4E_k(1+\lambda_n)}; \quad b_n^{(k)} = \frac{1+\nu_k}{E_k(1+\lambda_n)}; \quad c_n^{(k)} = \frac{\lambda_n(1+\nu_k)+4}{4E_k(1+\lambda_n)} \tag{40}$$

$$\mathbf{F}_c^{(k)} = \begin{bmatrix} \cos 2\theta & \sin 2\theta & \frac{\theta}{2} & \frac{1}{2} & 0 \\ -\cos 2\theta & -\sin 2\theta & \frac{\theta}{2} & \frac{1}{2} & 0 \\ -\sin 2\theta & \cos 2\theta & -\frac{1}{4} & 0 & 0 \end{bmatrix} \tag{41}$$

and

$$\mathbf{G}_c^{(k)} = \begin{bmatrix} \frac{1+\nu_k}{E_k}\cos 2\theta & \frac{1+\nu_k}{E_k}\sin 2\theta & \frac{1-\nu_k}{2E_k}\theta & \frac{1-\nu_k}{4E_k} & 0 \\ -\frac{1+\nu_k}{E_k}\sin 2\theta & \frac{1+\nu_k}{E_k}\cos 2\theta & \frac{1}{E_k}\ln r & 0 & -1 \end{bmatrix} \tag{42}$$

The mechanical and thermal components of the stress and displacement vectors can be rewritten in terms of real variables as

$${}_\lambda{}^m\boldsymbol{\sigma}_p^{(k)} = \sum_{n=0}^{N}\sum_{r=1+\delta_{n0}}^{R_n}\hat{\mathbf{F}}_{nr}^{(k)m}\hat{\boldsymbol{\alpha}}_{nr} \quad \text{and} \quad {}_\lambda{}^m\mathbf{u}_p^{(k)} = \sum_{n=0}^{N}\sum_{r=1+\delta_{n0}}^{R_n}\hat{\mathbf{G}}_{nr}^{(k)m}\hat{\boldsymbol{\alpha}}_{nr} \tag{43}$$

$${}_\lambda{}^t\boldsymbol{\sigma}_p^{(k)} = \sum_{n=0}^{N}\sum_{r=1+\delta_{n0}}^{R_n}\hat{\mathbf{F}}_{nr}^{(k)t}\hat{\boldsymbol{\alpha}}_{nr} \quad \text{and} \quad {}_\lambda{}^t\mathbf{u}_p^{(k)} = \sum_{n=0}^{N}\sum_{r=1+\delta_{n0}}^{R_n}\hat{\mathbf{G}}_{nr}^{(k)t}\hat{\boldsymbol{\alpha}}_{nr} \tag{44}$$

$${}_c{}^t\boldsymbol{\sigma}_p^{(k)} = \mathbf{F}_c^{(k)}\mathbf{q}_c \quad \text{and} \quad {}_c{}^t\mathbf{u}_p^{(k)} = \mathbf{G}_c^{(k)}\mathbf{q}_c^{(k)} + r\kappa_k T_0\mathbf{e}_r \tag{45}$$

where the real matrices of order (3×2), $\hat{\mathbf{F}}_{nr}^{(k)}$ and $\hat{\mathbf{G}}_{nr}^{(k)}$, and the real vectors, ${}^m\hat{\boldsymbol{\alpha}}_{nt}$ and ${}^t\hat{\boldsymbol{\alpha}}_{nt}$, of order 2 are defined by

$$\hat{\mathbf{F}}_{nr}^{(k)} = \left[\operatorname{Re}\left\{\mathbf{F}_n^{(k)}\hat{\mathbf{q}}_{nr}^{(k)}\right\} \vdots -\operatorname{Im}\left\{\mathbf{F}_n^{(k)}\hat{\mathbf{q}}_{nr}^{(k)}\right\}\right] \tag{46}$$

$$\hat{\mathbf{G}}_{nr}^{(k)} = \left[\operatorname{Re}\left\{\mathbf{G}_n^{(k)}\hat{\mathbf{q}}_{nr}^{(k)}\right\} \vdots -\operatorname{Im}\left\{\mathbf{G}_n^{(k)}\hat{\mathbf{q}}_{nr}^{(k)}\right\}\right] \tag{47}$$

and

$${}^m\hat{\boldsymbol{\alpha}}_{nr}^T = \{\operatorname{Re}({}^m\alpha_{nr}), \operatorname{Im}({}^m\alpha_{nr})\} \tag{48}$$

$${}^t\hat{\boldsymbol{\alpha}}_{nr}^T = \{\operatorname{Re}({}^t\alpha_{nr}), \operatorname{Im}({}^t\alpha_{nr})\} \tag{49}$$

By defining the matrices and vectors in the form

$$\hat{\mathbf{F}}_n^{(k)} = \left[\hat{\mathbf{F}}_{n(1+\delta_{n0})}^{(k)} \vdots \hat{\mathbf{F}}_{n(2+\delta_{n0})}^{(k)} \vdots \cdots \vdots \hat{\mathbf{F}}_{nR_n}^{(k)}\right], \quad \hat{\mathbf{G}}_n^{(k)} = \left[\hat{\mathbf{G}}_{n(1+\delta_{n0})}^{(k)} \vdots \hat{\mathbf{G}}_{n(2+\delta_{n0})}^{(k)} \vdots \cdots \vdots \hat{\mathbf{G}}_{nR_n}^{(k)}\right] \tag{50}$$

$${}^m\hat{\boldsymbol{\alpha}}_n^T = \left\{{}^m\hat{\boldsymbol{\alpha}}_{n(1+\delta_{n0})}^T, {}^m\hat{\boldsymbol{\alpha}}_{n(2+\delta_{n0})}^T, \ldots, {}^m\hat{\boldsymbol{\alpha}}_{nR_n}^T\right\}, \quad {}^t\hat{\boldsymbol{\alpha}}_n^T = \left\{{}^t\hat{\boldsymbol{\alpha}}_{n(1+\delta_{n0})}^T, {}^t\hat{\boldsymbol{\alpha}}_{n(2+\delta_{n0})}^T, \ldots, {}^t\hat{\boldsymbol{\alpha}}_{nR_n}^T\right\} \tag{51}$$

the mechanical and thermal components of the stress and displacements can be rewritten in a concise form as

$$ {}_{\lambda}{}^{m}\boldsymbol{\sigma}_{p}^{(k)} = \sum_{n=0}^{N} \hat{\mathbf{F}}_{n}^{(k)m}\hat{\boldsymbol{\alpha}}_{n} \quad \text{and} \quad {}_{\lambda}{}^{m}\mathbf{u}_{p}^{(k)} = \sum_{n=0}^{N} \hat{\mathbf{G}}_{n}^{(k)m}\hat{\boldsymbol{\alpha}}_{n} \tag{52} $$

$$ {}_{\lambda}{}^{t}\boldsymbol{\sigma}_{p}^{(k)} = \sum_{n=0}^{N} \hat{\mathbf{F}}_{n}^{(k)\mathrm{t}}\hat{\boldsymbol{\alpha}}_{n} \quad \text{and} \quad {}_{\lambda}{}^{t}\mathbf{u}_{p}^{(k)} = \sum_{n=0}^{N} \hat{\mathbf{G}}_{n}^{(k)\mathrm{t}}\hat{\boldsymbol{\alpha}}_{n} \tag{53} $$

$$ {}_{c}{}^{t}\boldsymbol{\sigma}_{p}^{(k)} = \mathbf{F}_{c}^{(k)}\mathbf{q}_{c} \quad \text{and} \quad {}_{c}{}^{t}\mathbf{u}_{p}^{(k)} = \mathbf{G}_{c}^{(k)}\mathbf{q}_{c}^{(k)} + r\kappa_{k}T_{0}\mathbf{e}_{r} \tag{54} $$

2.2. Global element stiffness matrix

The stiffness matrix for the global element of multiple dissimilar materials under mechanical and thermal loading is obtained by considering the total potential expressed in the form

$$ \pi = \left\{ \frac{1}{2}\int_{A_k} C_{\alpha\beta\gamma\eta}^{(k)}\varepsilon_{\alpha\beta}^{(k)}\varepsilon_{\gamma\eta}^{(k)}\,\mathrm{d}A - \int_{A_k} C_{\alpha\beta\gamma\eta}^{(k)}\,{}^{\circ}\varepsilon_{\alpha\beta}^{(k)}\varepsilon_{\gamma\eta}^{(k)}\,\mathrm{d}A - \int_{\hat{\Gamma}_k} \hat{t}_{\alpha}^{(k)}(u_{\alpha}^{(k)} - \hat{u}_{\alpha}^{k})\,\mathrm{d}\Gamma - \int_{\hat{\Gamma}_k} {}^{*}t_{\alpha}^{k}\hat{u}_{\alpha}^{(k)},\,\mathrm{d}\Gamma \right\} \tag{55} $$

with $\alpha,\ \beta,\ \gamma,\ \eta = x, y$. Non-stress-producing strain components in each material sector due to uniform temperature variation, T_0, are denoted by ${}^{\circ}\varepsilon_{\alpha\beta}^{(k)}$ and defined as

$$ {}^{\circ}\varepsilon_{\alpha\beta}^{(k)} = \kappa^{(k)}T_{0}\delta_{\alpha\beta} \tag{56} $$

The total strain components, $\varepsilon_{\alpha\beta}^{(k)}$, are decomposed as

$$ \varepsilon_{\alpha\beta}^{(k)} = {}_{\lambda}{}^{m}\varepsilon_{\alpha\beta}^{(k)} + {}_{\lambda+c}{}^{t}\varepsilon_{\alpha\beta}^{(k)} \tag{57} $$

in which ${}_{\lambda}{}^{m}\varepsilon_{\alpha\beta}^{(k)}$ represents the unknown strain components due to mechanical loading only and ${}_{\lambda+c}{}^{t}\varepsilon_{\alpha\beta}^{(k)}$ represents the known initial strain components arising from uniform temperature variation, T_0, in a domain of multiple dissimilar material sectors. The corresponding displacement components are given by

$$ u_{\alpha}^{(k)} = {}_{\lambda}{}^{m}u_{\alpha}^{(k)} + {}_{\lambda+c}{}^{t}u_{\alpha}^{(k)} \tag{58} $$

The left superscripts m and t denote the contributions associated with mechanical and thermal loading, respectively. The left subscript λ represents the deformations corresponding to homogeneous (eigen) system whereas the left subscript $\lambda + c$ represents the deformations corresponding to both homogeneous and complementary solutions.

With the material property tensor for each sector specified by

$$ C_{\alpha\beta\gamma\eta}^{(k)} = \frac{E_k}{(1+\nu_k)}\delta_{\gamma\alpha}\delta_{\eta\beta} + \frac{\nu_k E_k}{(1+\nu_k)(1-2\nu_k)}\delta_{\alpha\beta}\delta_{\gamma\eta} \tag{59} $$

the stress components due to mechanical and thermal loading are obtained from

$$ {}_{\lambda}{}^{m}\sigma_{\alpha\beta}^{(k)} = C_{\alpha\beta\gamma\eta}^{(k)}\,{}_{\lambda}{}^{m}\varepsilon_{\gamma\eta}^{(k)} \tag{60} $$

$$ {}_{\lambda+c}{}^{t}\sigma_{\alpha\beta}^{(k)} = C_{\alpha\beta\gamma\eta}^{(k)}\left({}_{\lambda+c}{}^{t}\varepsilon_{\gamma\eta}^{(k)} - {}^{\circ}\varepsilon_{\gamma\eta}^{(k)}\right) \tag{61} $$

The total (actual) stress components, $\sigma_{\alpha\beta}^{(k)}$, can be decomposed as

$$ \sigma_{\alpha\beta}^{(k)} = {}_{\lambda}{}^{m}\sigma_{\alpha\beta}^{(k)} + {}_{\lambda+c}{}^{t}\sigma_{\alpha\beta}^{(k)} \tag{62} $$

The unknown components of traction and displacement vectors along the common boundary segments, $\hat{\Gamma}_k$ (shown in Fig. 2), are denoted by $\hat{t}_\alpha^k$ and $\hat{u}_\alpha^k$. These traction components can be decomposed as

$$\hat{t}_\alpha^{(k)} = {}_\lambda{}^m\hat{t}_\alpha^{(k)} + {}_{\lambda+c}{}^t\hat{t}_\alpha^{(k)} \tag{63}$$

in which

$${}_\lambda{}^m\hat{t}_\alpha^{(k)} = {}_\lambda{}^m\sigma_{\alpha\beta}^{(k)}\hat{n}_\beta^{(k)} \quad \text{and} \quad {}_{\lambda+c}{}^t\hat{t}_\alpha^{(k)} = {}_{\lambda+c}{}^t\sigma_{\alpha\beta}^{(k)}\hat{n}_\beta^{(k)} \tag{64}$$

The known applied traction components along the common boundary segments are represented by ${}^*t_\alpha^{(k)}$.

Substituting for the total strain components from Eq. (57) along with the strain–displacement relations in the expression for the total potential, Eq. (55) and applying the divergence theorem while invoking the automatic satisfaction of the equilibrium equations in each sector reduces the total potential expression to

$$\begin{aligned}\pi = &\sum_{k=1}^{K}\left\{\frac{1}{2}\int_{\Gamma_k} {}_\lambda{}^m\sigma_{\alpha\beta}^{(k)}\,{}_\lambda{}^m u_\alpha^{(k)} n_\beta^{(k)}\,\mathrm{d}\Gamma + \int_{\Gamma_k} {}_{\lambda+c}{}^t\sigma_{\alpha\beta}^{(k)}\,{}_\lambda{}^m u_\alpha^{(k)} n_\beta^{(k)}\,\mathrm{d}\Gamma\right\}\\ &-\sum_{k=1}^{K}\left\{\int_{\hat{\Gamma}_k}\hat{t}_\alpha^{(k)}\,{}_{\lambda+c}{}^t u_\alpha^{(k)}\,\mathrm{d}\Gamma + \int_{\hat{\Gamma}_k}\hat{t}_\alpha^{(k)}\left({}_\lambda{}^m u_\alpha^{(k)} - \hat{u}_\alpha^{(k)}\right)\mathrm{d}\Gamma + \int_{\hat{\Gamma}_k}{}^*t_\alpha^{(k)}\hat{u}_\alpha^{(k)}\,\mathrm{d}\Gamma\right\} + \pi_0\end{aligned} \tag{65}$$

in which π_0 represents the total potential associated with the known initial strain and stress components arising from thermal loading only

$$\pi_0 = \sum_{k=1}^{K}\left\{\frac{1}{2}\int_{\Gamma_k} {}^t_{\lambda+c}\sigma_{\alpha\beta}^{(k)}\,{}_{\lambda+c}{}^t u_\alpha^{(k)} n_\beta^{(k)}\,\mathrm{d}\Gamma - \frac{1}{2}\int_{\Gamma_k} C_{\alpha\beta\gamma\eta}^{(k)}\,{}^\circ\varepsilon_{\gamma\eta}^{(k)}\,{}_{\lambda+c}{}^t u_\alpha^{(k)} n_\beta^{(k)}\,\mathrm{d}\Gamma\right\} \tag{66}$$

Because the initial strain and the corresponding initial stresses in this expression are known from the solution for thermal loading only (described in Appendix B), its first variation automatically vanishes, i.e., $\delta\pi_0 = 0$.

The boundary integrals describing each sector Γ_k can be decomposed as

$$\begin{aligned}\sum_{k=1}^{K}\int_{\Gamma_k} {}_\lambda{}^m\sigma_{\alpha\beta}^{(k)}\,{}_\lambda{}^m u_\alpha^{(k)} n_\beta^{(k)}\,\mathrm{d}\Gamma = &\sum_{k=1}^{K-1}\left\{\int_{\tilde{\Gamma}_k} {}_\lambda{}^m\sigma_{\alpha\beta}^{(k)}\,{}_\lambda{}^m u_\alpha^{(k)}\tilde{n}_\beta^{(k)}\,\mathrm{d}\Gamma + \int_{\overline{\Gamma}_{k+1}} {}_\lambda{}^m\sigma_{\alpha\beta}^{(k+1)}\,{}_\lambda{}^m u_\alpha^{(k+1)}\bar{n}_\beta^{(k+1)}\,\mathrm{d}\Gamma\right\}\\ &+\int_{\tilde{\Gamma}_K} {}_\lambda{}^m\sigma_{\alpha\beta}^{(K)}\,{}_\lambda{}^m u_\alpha^{(K)}\tilde{n}_\beta^{(K)}\,\mathrm{d}\Gamma + \int_{\overline{\Gamma}_1} {}_\lambda{}^m\sigma_{\alpha\beta}^{(1)}\,{}_\lambda{}^m u_\alpha^{(1)}\bar{n}_\beta^{(1)}\,\mathrm{d}\Gamma\\ &+\sum_{k=1}^{K}\int_{\hat{\Gamma}_k} {}_\lambda{}^m\sigma_{\alpha\beta}^{(k)}\,{}_\lambda{}^m u_\alpha^{(k)}\hat{n}_\beta^{(k)}\,\mathrm{d}\Gamma\end{aligned} \tag{67}$$

The continuity conditions between the adjacent sectors require that

$${}_\lambda{}^m\tilde{u}_\alpha^{(k)} = {}_\lambda{}^m\bar{u}_\alpha^{(k+1)} \tag{68}$$

$${}_\lambda{}^m\sigma_{\alpha\beta}^{(k)}\tilde{n}_\alpha^{(k)} = -{}_\lambda{}^m\sigma_{\alpha\beta}^{(k+1)}\bar{n}_\alpha^{(k+1)} \tag{69}$$

with $k = 1, \ldots, K-1$. For a closed junction, the additional continuity conditions are

$${}_\lambda{}^m\tilde{u}_\alpha^{(K)} = {}_\lambda{}^m\bar{u}_\alpha^{(1)} \tag{70}$$

$${}_\lambda{}^m\sigma_{\alpha\beta}^{(K)}\tilde{n}_\alpha^{(K)} = -{}_\lambda{}^m\sigma_{\alpha\beta}^{(1)}\bar{n}_\alpha^{(1)} \tag{71}$$

In the presence of an open junction with traction-free surfaces, the additional continuity equations are replaced by

$$ {}_{\lambda}{}^{m}\sigma_{\alpha\beta}^{(K)}\tilde{n}_{\alpha}^{(K)} = {}_{\lambda}{}^{m}\sigma_{\alpha\beta}^{(1)}\bar{n}_{\alpha}^{(1)} = 0 \tag{72} $$

Enforcing these conditions and noting that the adjacent boundaries are related to each other by $\widetilde{\Gamma}_k = \overline{\Gamma}_{k+1}$ and $\widetilde{\Gamma}_K = \overline{\Gamma}_1$, the expression for the potential energy becomes

$$ \begin{aligned} \pi = \sum_{k=1}^{K}\Bigg\{ & \frac{1}{2}\int_{\hat{\Gamma}_k} {}_{\lambda}{}^{m}\sigma_{\alpha\beta}^{(k)}\,{}_{\lambda}{}^{m}u_{\alpha}^{(k)}\hat{n}_{\beta}^{(k)}\,\mathrm{d}\Gamma + \int_{\hat{\Gamma}_k} {}_{\lambda+c}{}^{t}\sigma_{\alpha\beta}^{(k)}\,{}_{\lambda}{}^{m}u_{\alpha}^{(k)}\hat{n}_{\beta}^{(k)}\,\mathrm{d}\Gamma\Bigg\} \\ & - \sum_{k=1}^{K}\Bigg\{ \int_{\hat{\Gamma}_k} \hat{t}_{\alpha}^{(k)}\,{}_{\lambda+c}{}^{t}u_{\alpha}^{(k)}\,\mathrm{d}\Gamma + \int_{\hat{\Gamma}_k} \hat{t}_{\alpha}^{(k)}({}_{\lambda}{}^{m}u_{\alpha}^{(k)} - \hat{u}_{\alpha}^{(k)})\,\mathrm{d}\Gamma + \int_{\hat{\Gamma}_k} {}^{*}t_{\alpha}^{(k)}\hat{u}_{\alpha}^{(k)}\,\mathrm{d}\Gamma\Bigg\} + \pi_0 \end{aligned} \tag{73} $$

Substituting from Eqs. (63) and (64) into $\hat{t}_{\alpha}^{(k)}$ and invoking the condition that thermal stresses do not induce boundary tractions, ${}_{\lambda+c}{}^{t}\hat{t}_{\alpha}^{(k)} = {}_{\lambda+c}{}^{t}\sigma_{\alpha\beta}^{(k)}\hat{n}_{\beta}^{(k)} = 0$ as derived in Appendix B results in the matrix representation of the total potential in the form

$$ \begin{aligned} \pi = \sum_{k=1}^{K}\Bigg\{ & -\frac{1}{2}\int_{\hat{\Gamma}_k} {}_{\lambda}{}^{m}\boldsymbol{\sigma}^{(k)^T}\hat{\mathbf{n}}^{(k)^T}\,{}_{\lambda}{}^{m}\mathbf{u}^{(k)}\,\mathrm{d}\Gamma - \int_{\hat{\Gamma}_k} {}_{\lambda}{}^{m}\boldsymbol{\sigma}^{(k)^T}\hat{\mathbf{n}}^{(k)^T}\,{}_{\lambda+c}{}^{t}\mathbf{u}^{(k)}\,\mathrm{d}\Gamma \\ & + \int_{\hat{\Gamma}_k} {}_{\lambda}{}^{m}\boldsymbol{\sigma}^{(k)^T}\hat{\mathbf{n}}^{(k)^T}\hat{\mathbf{u}}^{(k)}\,\mathrm{d}\Gamma - \int_{\hat{\Gamma}_k} {}^{*}\mathbf{t}^{(k)}\hat{\mathbf{u}}^{(k)}\,\mathrm{d}\Gamma\Bigg\} + \pi_0 \end{aligned} \tag{74} $$

in which the vectors ${}_{\lambda}{}^{m}\boldsymbol{\sigma}^{(k)}$, ${}_{\lambda}{}^{m}\mathbf{u}^{(k)}$, ${}_{\lambda+c}{}^{t}\mathbf{u}^{(k)}$, ${}^{*}\mathbf{t}^{(k)}$, and $\hat{\mathbf{u}}^{(k)}$ are defined as

$$ {}_{\lambda}{}^{m}\boldsymbol{\sigma}^{(k)^T} = \left\{ {}_{\lambda}{}^{m}\sigma_{xx}^{(k)}, {}_{\lambda}{}^{m}\sigma_{yy}^{(k)}, {}_{\lambda}{}^{m}\sigma_{xy}^{(k)} \right\} \tag{75} $$

$$ {}_{\lambda}{}^{m}\mathbf{u}^{(k)^T} = \left\{ {}_{\lambda}{}^{m}u_{x}^{(k)}, {}_{\lambda}{}^{m}u_{y}^{(k)} \right\} \tag{76} $$

$$ {}_{\lambda+c}{}^{t}\mathbf{u}^{(k)^T} = \left\{ {}_{\lambda+c}{}^{t}u_{x}^{(k)}, {}_{\lambda+c}{}^{t}u_{y}^{(k)} \right\} \tag{77} $$

$$ {}^{*}\mathbf{t}^{(k)^T} = \left\{ {}^{*}t_{x}^{(k)}, {}^{*}t_{y}^{(k)} \right\} \tag{78} $$

$$ \hat{\mathbf{u}}^{(k)^T} = \left\{ \hat{u}_{x}^{(k)}, \hat{u}_{y}^{(k)} \right\} \tag{79} $$

and the matrix $\hat{\mathbf{n}}^{(k)}$ contains the components of the unit normal along $\hat{\Gamma}_k$

$$ \hat{\mathbf{n}}^{(k)^T} = \begin{bmatrix} \hat{n}_{x}^{(k)} & 0 \\ 0 & \hat{n}_{y}^{(k)} \\ \hat{n}_{y}^{(k)} & \hat{n}_{x}^{(k)} \end{bmatrix} \tag{80} $$

Introduce the transformation matrices, $\mathbf{Z}_{\sigma}^{(k)}$ and $\mathbf{Z}_{u}^{(k)}$, given by

$$ \mathbf{Z}_{\sigma}^{(k)} = \begin{bmatrix} (\hat{n}_{x}^{(k)})^2 & (\hat{n}_{y}^{(k)})^2 & -2\hat{n}_{x}^{(k)}\hat{n}_{y}^{(k)} \\ (\hat{n}_{y}^{(k)})^2 & (\hat{n}_{x}^{(k)})^2 & 2\hat{n}_{x}^{(k)}\hat{n}_{y}^{(k)} \\ \hat{n}_{x}^{(k)}\hat{n}_{y}^{(k)} & -\hat{n}_{x}^{(k)}\hat{n}_{y}^{(k)} & (\hat{n}_{x}^{(k)})^2 - (\hat{n}_{y}^{(k)})^2 \end{bmatrix} \tag{81} $$

and

$$\mathbf{Z}_u^{(k)} = \begin{bmatrix} \hat{n}_x^{(k)} & -\hat{n}_y^{(k)} \\ \hat{n}_y^{(k)} & \hat{n}_x^{(k)} \end{bmatrix} \tag{82}$$

With these transformation matrices, the vectors of stress and displacement components can be rewritten as

$${}_{\lambda}{}^{m}\boldsymbol{\sigma}^{(k)} = \mathbf{Z}_\sigma^{(k)}\,{}_{\lambda}{}^{m}\boldsymbol{\sigma}_p^{(k)} \tag{83}$$

$${}_{\lambda}{}^{m}\mathbf{u}^{(k)} = \mathbf{Z}_u^{(k)}\,{}_{\lambda}{}^{m}\mathbf{u}_p^{(k)} \tag{84}$$

$${}_{\lambda+c}{}^{t}\mathbf{u}^{(k)} = \mathbf{Z}_u^{(k)}\,{}_{\lambda+c}{}^{t}\mathbf{u}_p^{(k)} \tag{85}$$

and their substitution in the total potential results in

$$\begin{aligned}\pi = \sum_{k=1}^{K}\left\{ -\frac{1}{2}\int_{\hat{\Gamma}_k} {}_{\lambda}{}^{m}\boldsymbol{\sigma}_p^{(k)^T}\mathbf{Z}_\sigma^{(k)^T}\hat{\mathbf{n}}^{(k)}\mathbf{Z}_u^{(k)}\,{}_{\lambda}{}^{m}\mathbf{u}_p^{(k)}\,\mathrm{d}\Gamma - \int_{\hat{\Gamma}_k} {}_{\lambda}{}^{m}\boldsymbol{\sigma}_p^{(k)^T}\mathbf{Z}_\sigma^{(k)^T}\hat{\mathbf{n}}^{(k)}\mathbf{Z}_u^{(k)}\,{}_{\lambda+c}{}^{t}\mathbf{u}_p^{(k)}\,\mathrm{d}\Gamma \right\} \\ + \sum_{k=1}^{K}\left\{ \int_{\hat{\Gamma}_k} {}_{\lambda}{}^{m}\boldsymbol{\sigma}_p^{(k)^T}\mathbf{Z}_\sigma^{(k)^T}\hat{\mathbf{n}}^{(k)}\hat{\mathbf{u}}^{(k)}\,\mathrm{d}\Gamma - \int_{\hat{\Gamma}_k} \hat{\mathbf{u}}^{(k)^T*}\mathbf{t}^{(k)}\,\mathrm{d}\Gamma \right\} + \pi_0\end{aligned} \tag{86}$$

The vector of displacement components, $\hat{\mathbf{u}}^{(k)}$, along the common boundary between the global element and the conventional elements can be expressed in terms of the nodal displacements of the conventional elements as

$$\hat{\mathbf{u}}^{(k)} = \hat{\boldsymbol{\Lambda}}^{(k)}\hat{\mathbf{v}} \tag{87}$$

in which the matrix $\hat{\boldsymbol{\Lambda}}^{(k)}$ contains the linear interpolation function compatible with those of the conventional elements. The vector $\hat{\mathbf{v}}$ contains the nodal degrees of freedom associated with the conventional elements located on the boundary segment $\hat{\Gamma}_k$.

Substituting for ${}_{\lambda}{}^{m}\boldsymbol{\sigma}_p^{(k)}$, ${}_{\lambda}{}^{m}\mathbf{u}_p^{(k)}$, and $\hat{\mathbf{u}}^{(k)}$ from Eqs. (52) and (87) in the expression for the total potential leads to

$$\pi = -\frac{1}{2}\sum_{k=1}^{K} {}^{m}\hat{\boldsymbol{\alpha}}^{T}\mathbf{H}^{(k)}\,{}^{m}\hat{\boldsymbol{\alpha}} - \sum_{k=1}^{K} {}^{m}\hat{\boldsymbol{\alpha}}^{T}\,{}^{t}\mathbf{f}^{(k)} + \sum_{k=1}^{K} {}^{m}\hat{\boldsymbol{\alpha}}^{T}\mathbf{R}^{(k)}\mathbf{v} - \sum_{k=1}^{K}\mathbf{v}^{T*}\mathbf{f}^{(k)} + \pi_0 \tag{88}$$

in which

$${}^{m}\hat{\boldsymbol{\alpha}}^{T} = \left\{ {}^{m}\hat{\boldsymbol{\alpha}}_0^{T}, {}^{m}\hat{\boldsymbol{\alpha}}_1^{T}, {}^{m}\hat{\boldsymbol{\alpha}}_2^{T}, \ldots, {}^{m}\hat{\boldsymbol{\alpha}}_N^{T} \right\} \tag{89}$$

and

$$\mathbf{H}^{(k)} = \begin{bmatrix} \mathbf{H}_{00}^{(k)} & \mathbf{H}_{01}^{(k)} & \cdots & \mathbf{H}_{0N}^{(k)} \\ \mathbf{H}_{10}^{(k)} & \mathbf{H}_{11}^{(k)} & \cdots & \mathbf{H}_{1N}^{(k)} \\ \vdots & \vdots & & \vdots \\ \mathbf{H}_{N0}^{(k)} & \mathbf{H}_{N1}^{(k)} & \cdots & \mathbf{H}_{NN}^{(k)} \end{bmatrix} \quad \text{with } \mathbf{H}_{ij}^{(k)} = \int_{\hat{\Gamma}_k} \hat{\mathbf{F}}_i^{(k)^T}\mathbf{Z}_\sigma^{(k)^T}\hat{\mathbf{n}}^{(k)}\mathbf{Z}_u^{(k)}\hat{\mathbf{G}}_j^{(k)}\,\mathrm{d}\Gamma \tag{90}$$

$${}^{t}\mathbf{f}^{(k)^T} = \left\{ {}^{t}\mathbf{f}_0^{(k)^T}, {}^{t}\mathbf{f}_1^{(k)^T}, {}^{t}\mathbf{f}_2^{(k)^T}, \ldots, {}^{t}\mathbf{f}_N^{(k)^T} \right\} \quad \text{with } {}^{t}\mathbf{f}_i^{(k)} = \int_{\hat{\Gamma}_k} \hat{\mathbf{F}}_i^{(k)^T}\mathbf{Z}_\sigma^{(k)^T}\hat{\mathbf{n}}^{(k)}\mathbf{Z}_u^{(k)}\,{}_{\lambda+c}{}^{t}\mathbf{u}_p^{(k)}\,\mathrm{d}\Gamma \tag{91}$$

$$\mathbf{R}^{(k)^T} = \left\{ \mathbf{R}_0^{(k)^T}, \mathbf{R}_1^{(k)^T}, \mathbf{R}_2^{(k)^T}, \ldots, \mathbf{R}_N^{(k)^T} \right\} \quad \text{with } \mathbf{R}_i^{(k)} = \int_{\hat{\Gamma}_k} \hat{\mathbf{F}}_i^{(k)^T} \mathbf{Z}_\sigma^{(k)^T} \hat{\mathbf{n}}^{(k)} \Lambda^{(k)} \, \mathrm{d}\Gamma \tag{92}$$

and

$${}^*\mathbf{f}^{(k)} = \int_{\hat{\Gamma}_k} \Lambda^{(k)^T} {}^*\mathbf{t}^{(k)} \, \mathrm{d}\Gamma \tag{93}$$

Defining

$$\mathbf{H} = \sum_{k=1}^{K} \mathbf{H}^{(k)}; \quad \mathbf{R} = \sum_{k=1}^{K} \mathbf{R}^{(k)}; \quad {}^t\mathbf{f} = \sum_{k=1}^{K} {}^t\mathbf{f}^{(k)}; \quad {}^*\mathbf{f} = \sum_{k=1}^{K} {}^*\mathbf{f}^{(k)} \tag{94}$$

permits the expression of the potential energy in its final form as

$$\pi = -\frac{1}{2} {}^m\hat{\boldsymbol{\alpha}}^T \mathbf{H} {}^m\hat{\boldsymbol{\alpha}} - {}^m\hat{\boldsymbol{\alpha}}^T {}^t\mathbf{f} + {}^m\hat{\boldsymbol{\alpha}}^T \mathbf{R}\mathbf{v} - \mathbf{v}^T {}^*\mathbf{f} + \pi_0 \tag{95}$$

The unknown vectors ${}^m\hat{\boldsymbol{\alpha}}$ and $\mathbf{v}$ represent the generalized coordinates associated with the mechanical deformations and the nodal displacements arising from both thermal and mechanical loading, respectively. In order to express the total potential in terms of one unknown vector, $\mathbf{v}$, the first variation of the total potential with respect to $\hat{\boldsymbol{\alpha}}$ is taken, leading to

$$\delta\pi = -\delta {}^m\hat{\boldsymbol{\alpha}}^T \left\{ \mathbf{H}' {}^m\hat{\boldsymbol{\alpha}} + {}^t\mathbf{f} - \mathbf{R}\mathbf{v} \right\} + \delta\pi_0 \tag{96}$$

in which

$$\mathbf{H}' = \tfrac{1}{2}\left\{ \mathbf{H} + \mathbf{H}^T \right\} = \mathbf{H} \tag{97}$$

where $\mathbf{H} = \mathbf{H}^T$ is based on Maxwell's reciprocal theorem. While noting that $\delta\pi_0 = 0$, enforcing the first variation with respect to ${}^m\hat{\boldsymbol{\alpha}}$ to vanish results in

$$\delta {}^m\hat{\boldsymbol{\alpha}}^T \left\{ \mathbf{H}' {}^m\hat{\boldsymbol{\alpha}} + {}^t\mathbf{f} - \mathbf{R}\mathbf{v} \right\} = 0 \tag{98}$$

Solution of this equation yields ${}^m\hat{\boldsymbol{\alpha}}$ in terms of the nodal displacement vector, $\mathbf{v}$, as

$${}^m\hat{\boldsymbol{\alpha}} = \mathbf{H}^{-1} \{ \mathbf{R}\mathbf{v} - {}^t\mathbf{f} \} \tag{99}$$

Substituting for ${}^m\hat{\boldsymbol{\alpha}}$ in the expression for the total potential leads to

$$\pi = \tfrac{1}{2}\mathbf{v}^T \mathbf{R}^T \mathbf{H}^{-1} \mathbf{R}\mathbf{v} - \mathbf{v}^T \mathbf{R}^T \mathbf{H}^{-1} {}^t\mathbf{f} - \mathbf{v}^T {}^*\mathbf{f} + \tfrac{1}{2} {}^t\mathbf{f}^T \mathbf{H}^{-1} {}^t\mathbf{f} + \pi_0 \tag{100}$$

Enforcing the first variation of the total potential to vanish results in the nodal equations of equilibrium for the global element as

$$\delta\pi = \mathbf{v}^T \{ \mathbf{K}\mathbf{v} - {}^t\mathbf{F} - {}^*\mathbf{f} \} = 0 \tag{101}$$

leading to

$$\mathbf{K}\mathbf{v} = {}^*\mathbf{f} + {}^t\mathbf{F} \tag{102}$$

in which $\mathbf{K}$ and ${}^t\mathbf{F}$ are defined as $\mathbf{K} = \mathbf{R}^T \mathbf{H}^{-1} \mathbf{R}$ and ${}^t\mathbf{F} = \mathbf{R}^T \mathbf{H}^{-1}$. The vector ${}^*\mathbf{f}$ represents the internal load vector at a node common to both the global and conventional elements. If a node is free of conventional elements, the components of the load vector represent the external force components. The vector ${}^t\mathbf{F}$ represents the reaction force that suppresses the deformation, resulting from thermal loading only, at the common nodes of global and conventional elements.

3. Numerical results

The validity of the solution method has been established by analyzing the bi-metal thermostat considered by Munz and Yang (1992), the bi-material plate with an interface crack investigated by Yuuki and Cho (1989), and the crack perpendicular to the interface of a bi-material strip reported by Gadi et al. (1995). In addition, a convergence study is conducted that assesses the present method's dependence on the global element size and number of eigenfunctions retained in the series representation of the stress and displacement fields. Finally, a circular bi-material inclusion embedded in a different material infinite in extent is considered under uniform temperature change.

3.1. Bi-metal thermostat

Although the present formulation permits combined mechanical and thermal loading, the bi-metal thermostat shown in Fig. 3 is considered under either mechanical or uniform temperature loading in order to compare the present stress field predictions with those of Munz and Yang (1992). As shown in Fig. 3, the parameters H_1, H_2, and L describe the loading and the geometry of the plate. The position of the global element surrounded by conventional elements in the finite element model is also shown in Fig. 3.

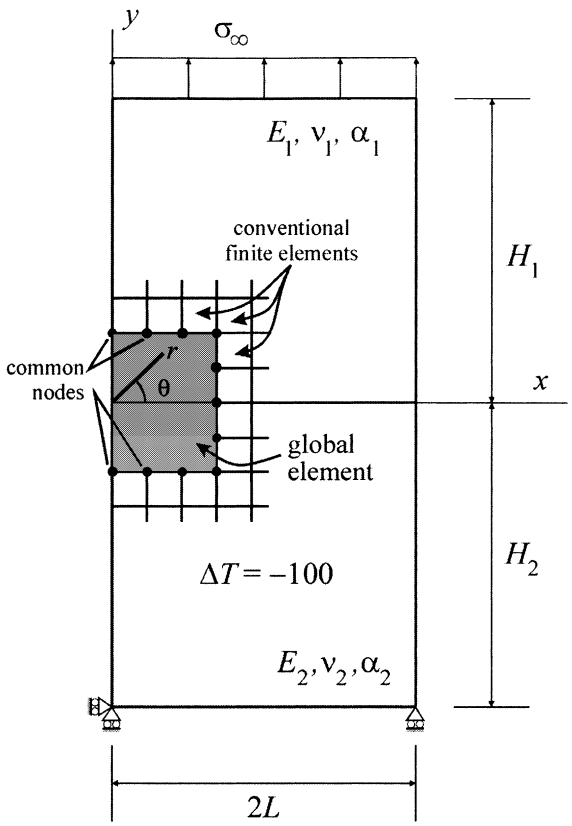

Fig. 3. Geometry and loading of a bi-metal thermostat.

The first and second materials have the same Poisson's ratio of $v_1 = v_2 = 0.2$. Their thermal expansion coefficients are specified as $\alpha_1 = 15 \times 10^{-6}$ K^{-1} and $\alpha_2 = 5 \times 10^{-6}$ K^{-1}. The first material has a Young's modulus of $E_1 = 280.0$ GPa. The Young's modulus of the second material varies as $E_2 = 14.737$, 31.111, 70.0, 120.0, 186.67 GPa. The geometry is defined by $H_1/L = H_2/L = 2$. The applied stress, σ_0, in the direction perpendicular to the interface is unity, and the applied uniform temperature change is $\Delta T = -100$ K.

Under plane strain conditions, the present results are also compared against the finite element analysis predictions with an extremely refined mesh of only conventional elements using ANSYS, a commercially available finite element analysis program. In the finite element analysis with conventional elements only, the sub-modeling feature of ANSYS is utilized to achieve acceptable mesh refinement near the junction. The model consisted of 20,000 elements. In the sub-modeling phase, three times the region of the global element is modeled using, again, 20,000 elements.

The comparison of the results for the tangential stress along the interface near the open junction is presented in Figs. 4–6. The results concerning mechanical loading are presented in Fig. 4. The results concerning uniform temperature and two different plate sizes are shown in Figs. 5 and 6. As observed in these figures, the predictions from the present analysis and the finite element analysis with an extremely refined mesh are in remarkable agreement up to a very small distance away from the junction point. As is well known, the results of the conventional finite element analysis suffer from accuracy at a point very close to the junction.

The agreement between the present analysis results and those of Munz and Yang (1992) improves as the junction point is approached because both analyses include the leading-order term of the asymptotic solution. However, the solution reported by Munz and Yang (1992) loses its accuracy away from the junction point because it is based on a relationship, obtained through curve fitting of a fifth-order polynomial, in terms of the leading order of the singular behavior, λ_1, as

$$\sigma_{\theta\theta}(r,0) = \frac{\bar{\sigma}}{(r/L)^{\lambda_1}} g(\lambda_1) \tag{103}$$

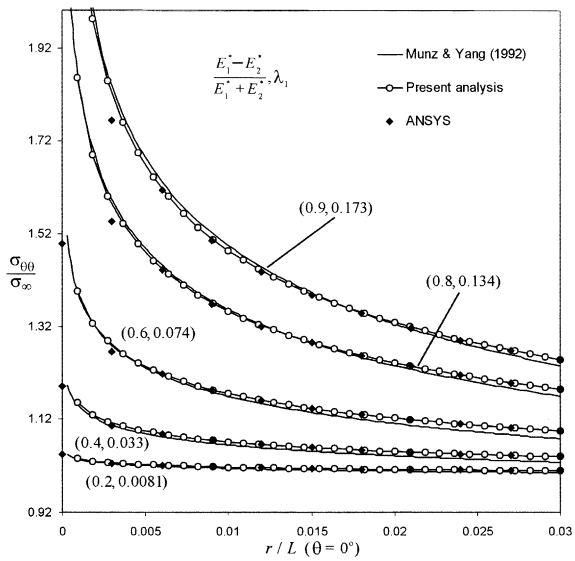

Fig. 4. Variation of the peeling stress away from the junction along the interface for different material combinations under mechanical loading.

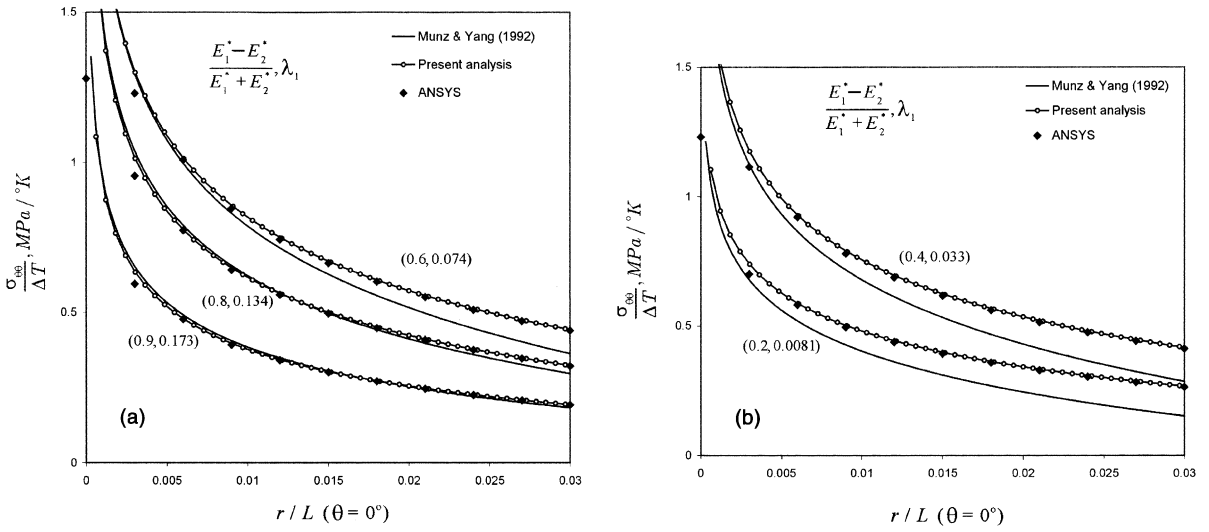

Fig. 5. Variation of the peeling stress away from the junction along the interface for different material combinations under thermal loading: (a) $\lambda_1 = 0.074$, 0.134, and 0.173; (b) $\lambda_1 = 0.0081$ and 0.033.

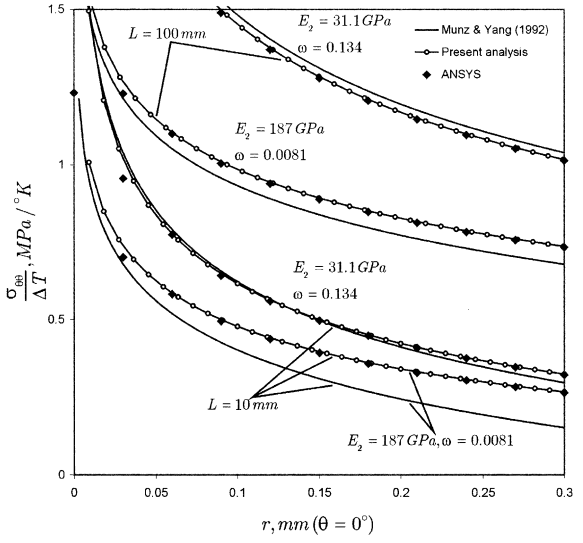

Fig. 6. Variation of the peeling stress away from the junction along the interface in a small and large plate of different material combinations under thermal loading.

with

$$g(\lambda_1) = 1 - 2.89\lambda_1 + 11.4\lambda_1^2 - 51.9\lambda_1^3 + 135.7\lambda_1^4 - 135.8\lambda_1^5 \tag{104}$$

where $\bar{\sigma} = \sigma_\infty$ for remote mechanical loading (no thermal loading) in the direction perpendicular to the interface and $\bar{\sigma} = \sigma_0[\{(r/L)^{\lambda_1}/g(\lambda_1)\} - 1]$ for thermal loading (no mechanical loading). Munz and Yang define σ_0 as

$$\sigma_0 = \Delta\alpha\,\Delta E\,\Delta T \tag{105}$$

where

$$\Delta\alpha = \alpha_1(1+\nu_1) - \alpha_2(1+\nu_2), \quad \Delta E = 1\Big/\left(\frac{1}{E_1^*} - \frac{1}{E_2^*}\right) \tag{106}$$

with $E_1^* = \nu_1(1+\nu_1)/E_1$ and $E_2^* = \nu_2(1+\nu_2)/E_2$. The coefficients of the polynomial are calculated by the finite element method.

The results reported by Munz and Yang (1992) deviate from the present analysis and ANSYS predictions significantly as the magnitude of the leading-order singular term decreases. Also, their results are sensitive to the size of the bi-metal thermostat, especially for small values of the leading-order singular term, as shown in Fig. 6.

3.2. Interface crack in dissimilar materials

In order to validate the stress intensity factors, K_1 and K_2, and the J-integral values, a finite geometry bi-material plate with an interface crack (Fig. 7) is considered. As assigned by Yuuki and Cho (1989), both materials have the same Poisson's ratio, $\nu_1 = \nu_2 = 0.3$, and the ratio of their Young's moduli, E_1/E_2, varies from 2 to 100. The center crack length-to-plate width ratio, $2a/W$, is specified as 0.1, 0.2, 0.3, 0.4, and 0.5, with $W = 10$ in.

The stress field along the interface near the crack tip can be described by

$$\sigma_{\theta\theta} - \mathrm{i}\sigma_{r\theta} = \lim_{r\to 0} \frac{K_1 + \mathrm{i}K_2}{\sqrt{2\pi}}\, r^{-\lambda_1}$$

in which the stress intensity factors, K_1 and K_2 are obtained from

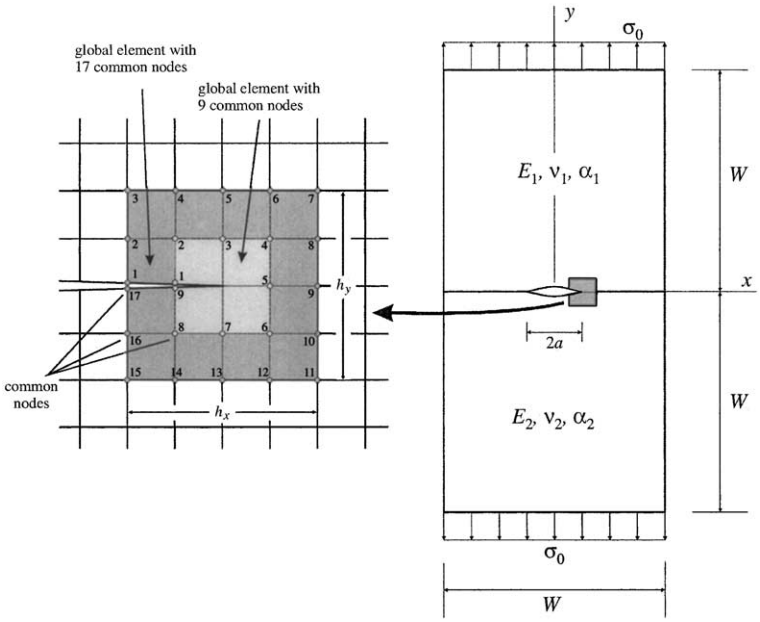

Fig. 7. A central bi-material interface crack in a finite geometry plate under uniform tension.

$$K_1 + iK_2 = \sqrt{2\pi}\{\mathrm{Re}[F_{\theta\theta}(\theta;\lambda_1)] - i\mathrm{Re}[F_{r\theta}(\theta;\lambda_1)]\}_{\theta=\pi}$$

J-integral calculations are based on the expression

$$J = \sum_{k=1}^{K} \int_{\theta_k}^{\theta_{k+1}} \left[U^{(k)} n_x^{(k)} - (t_x^{(k)} u_{x,x}^{(k)} + t_y^{(k)} u_{y,x}^{(k)}) + t_x^{(k)} \bar{\alpha}^{(k)} T \right] \varepsilon \, \mathrm{d}\theta$$

where $U^{(k)}$ is the strain energy density of the stress-producing strains, $t_\alpha^{(k)} = \sigma_{\alpha\beta}^{(k)} n_\beta^{(k)}$ $(\alpha, \beta = 1, 2)$ are the tractions along the boundary of the integration path, $u_{x,x}^{(k)}$ and $u_{y,x}^{(k)}$ are the partial displacements of the global element with respect to local x-coordinate evaluated along the path of integration, ε is a small radial distance between the junction and the circular path of integration, $\bar{\alpha}^{(k)}$ is the coefficient of thermal expansion associated with the kth sector, and T is the uniform temperature change within the global element.

For a plate subjected to unit uniform stress, $\sigma_0 = 1$ lb/in.^{2}, in the direction perpendicular to the interface and under plane stress conditions, the stress intensity factors and the J-integral values from the present analysis are compared with those of Yuuki and Cho (1989) in Tables 1 and 2. A schematic of the two

Table 1
Fracture parameters for a finite plate with an interface crack by using a global element of 9 common nodes

E_1/E_2	$2a/W$	$K_1/\sigma_0\sqrt{\pi a}$			$K_2/\sigma_0\sqrt{\pi a}$			J-Integral		
		Present analysis	Yuuki and Cho (1989)	Percent difference	Present analysis	Yuuki and Cho (1989)	Percent difference	Present analysis	Yuuki and Cho (1989)	Percent difference
2	0.1	0.99532	0.99642	0.11	0.07143	0.07174	0.43	1.15716	1.15979	0.23
	0.2	1.01556	1.02009	0.44	0.04415	0.04290	2.90	2.40160	2.42276	0.87
	0.3	1.04907	1.05461	0.53	0.02764	0.02838	2.60	3.83940	3.88021	1.05
	0.4	1.10030	1.10588	0.51	0.01562	0.01569	0.41	5.62862	5.68590	1.01
	0.5	1.17637	1.18298	0.56	0.00617	0.00693	11.02	8.04086	8.13147	1.11
3	0.1	0.98696	0.98913	0.22	0.10629	0.10781	1.41	1.00030	1.00500	0.47
	0.2	1.00902	1.01481	0.57	0.06521	0.06667	2.19	2.07568	2.09987	1.15
	0.3	1.04280	1.04916	0.61	0.04025	0.04179	3.68	3.31661	3.35753	1.22
	0.4	1.09347	1.10074	0.66	0.02506	0.02382	5.18	4.85709	4.92215	1.32
	0.5	1.16822	1.17596	0.66	0.00738	0.00951	22.42	6.92727	7.01948	1.31
4	0.1	0.98013	0.98260	0.25	0.12678	0.12872	1.51	0.91663	0.92164	0.54
	0.2	1.00364	1.00989	0.62	0.07736	0.07924	2.37	1.90186	1.92602	1.25
	0.3	1.03762	1.04485	0.69	0.04723	0.04899	3.59	3.03749	3.08033	1.39
	0.4	1.08781	1.09564	0.71	0.02506	0.02779	9.83	4.49441	4.50914	0.33
	0.5	1.16144	1.16996	0.73	0.00738	0.00965	23.50	6.32982	6.42324	1.45
10	0.1	0.96005	0.96252	0.26	0.17070	0.17325	1.47	0.75410	0.75858	0.59
	0.2	0.98772	0.99435	0.67	0.10307	0.10610	2.86	1.56432	1.58618	1.38
	0.3	1.02213	1.02992	0.76	0.06138	0.06540	6.15	2.49474	2.53398	1.55
	0.4	1.07069	1.07846	0.72	0.03037	0.03406	10.84	3.63971	3.69340	1.45
	0.5	1.14070	1.14895	0.72	0.00527	0.01000	47.28	5.16002	5.23520	1.44
100	0.1	0.93912	0.93992	0.09	0.20336	0.20490	0.75	0.64622	0.64771	0.23
	0.2	0.97071	0.97506	0.45	0.12247	0.12464	1.74	1.34000	1.35259	0.93
	0.3	1.00527	1.01120	0.59	0.07211	0.07524	4.17	2.13280	2.15887	1.21
	0.4	1.05178	1.05732	0.52	0.03428	0.03782	9.37	3.10028	3.13372	1.07
	0.5	1.11755	1.12398	0.57	0.00328	0.00623	47.32	4.37061	4.42112	1.14

Table 2
Fracture parameters for a finite plate with an interface crack by using a global element of 17 common nodes

E_1/E_2	$2a/W$	$K_1/\sigma_0\sqrt{\pi a}$			$K_2/\sigma_0\sqrt{\pi a}$			J-Integral		
		Present analysis	Yuuki and Cho (1989)	Percent difference	Present analysis	Yuuki and Cho (1989)	Percent difference	Present analysis	Yuuki and Cho (1989)	Percent difference
2	0.1	1.00062	0.99642	0.42	−0.07238	−0.07174	0.89	1.16961	1.15979	0.85
	0.2	1.02114	1.02009	0.10	−0.04502	−0.04290	4.94	2.42818	2.42276	0.22
	0.3	1.05493	1.05461	0.03	−0.02849	−0.02838	0.39	3.88255	3.88021	0.06
	0.4	1.10651	1.10588	0.06	−0.01647	−0.01569	4.99	5.69244	5.68590	0.12
	0.5	1.18308	1.18298	0.01	−0.00704	−0.00693	1.58	8.13288	8.13147	0.02
3	0.1	0.99326	0.98913	0.42	−0.10831	−0.10781	0.46	1.01341	1.00500	0.84
	0.2	1.01569	1.01481	0.09	−0.06720	−0.06667	0.80	2.10365	2.09987	0.18
	0.3	1.04981	1.04916	0.06	−0.04225	−0.04179	1.10	3.36181	3.35753	0.13
	0.4	1.10091	1.10074	0.02	−0.02402	−0.02382	0.84	4.92378	4.92215	0.03
	0.5	1.17625	1.17596	0.03	−0.00964	−0.00951	1.32	7.02303	7.01948	0.05
4	0.1	0.98709	0.98260	0.46	−0.12970	−0.12872	0.77	0.93018	0.92164	0.93
	0.2	1.01103	1.00989	0.11	−0.08030	−0.07924	1.34	1.93066	1.92602	0.24
	0.3	1.04539	1.04485	0.05	−0.05023	−0.04899	2.53	3.08386	3.08033	0.11
	0.4	1.09605	1.09564	0.04	−0.02817	−0.02779	1.38	4.51255	4.50914	0.08
	0.5	1.17031	1.16996	0.03	−0.01068	−0.00965	10.72	6.42726	6.42324	0.06
10	0.1	0.96763	0.96252	0.53	−0.17540	−0.17325	1.24	0.76699	0.75858	1.11
	0.2	0.99575	0.99435	0.14	−0.10789	−0.10610	1.69	1.59122	1.58618	0.32
	0.3	1.03055	1.02992	0.06	−0.06637	−0.06540	1.47	2.53740	2.53398	0.13
	0.4	1.07959	1.07846	0.10	−0.03560	−0.03406	4.49	3.70147	3.69340	0.22
	0.5	1.15024	1.14895	0.11	−0.01083	−0.01000	8.31	5.24704	5.23520	0.23
100	0.1	0.94561	0.93992	0.61	−0.20758	−0.20490	1.31	0.65599	0.64771	1.28
	0.2	0.97748	0.97506	0.25	−0.12674	−0.12464	1.69	1.35996	1.35259	0.54
	0.3	1.01229	1.01120	0.11	−0.07649	−0.07524	1.66	2.16389	2.15887	0.23
	0.4	1.05911	1.05732	0.17	−0.03885	−0.03782	2.71	3.14454	3.13372	0.35
	0.5	1.12534	1.12398	0.12	−0.00812	−0.00623	30.32	4.43191	4.42112	0.24

different global element configurations used in this study is given in Fig. 7. The first and second configurations have 9 and 17 common nodes, respectively, with the conventional finite elements as indicated in this figure. Also shown in Fig. 7, h_x and h_y denote the size of the global element in the x- and y-directions, respectively. The results presented in Table 1 are obtained with a global element having 9 common nodes with a size of $h_x = 0.01W$ and $h_y = 0.011W$. Table 2 presents results corresponding to a global element with 17 common nodes with a size of $h_x = 0.02W$ and $h_y = 0.022W$.

As tabulated in Tables 1 and 2, the present analysis results are not sensitive to the global element size, and they are in agreement with the values reported by Yuuki and Cho (1989). The numerical values for normalized parameters, F_1 and F_2, reported by Yuuki and Cho (1989) are converted by

$$K_1 = \sqrt{\frac{F_1^2\sigma_0^2(\pi a)}{1+F_2^2}}; \quad K_2 = \sqrt{\frac{F_1^2F_2^2\sigma_0^2(\pi a)}{1+F_2^2}} \tag{107}$$

In order to establish the accuracy of the stress intensity factor calculations from the present analysis, an infinite dissimilar plate with an interface crack, shown in Fig. 8, is also considered. The Young's modulus and Poisson's ratio for the first material are specified as $E_1 = 1$ lb/in.^{2} and $\nu_1 = 0.3$. The Young's

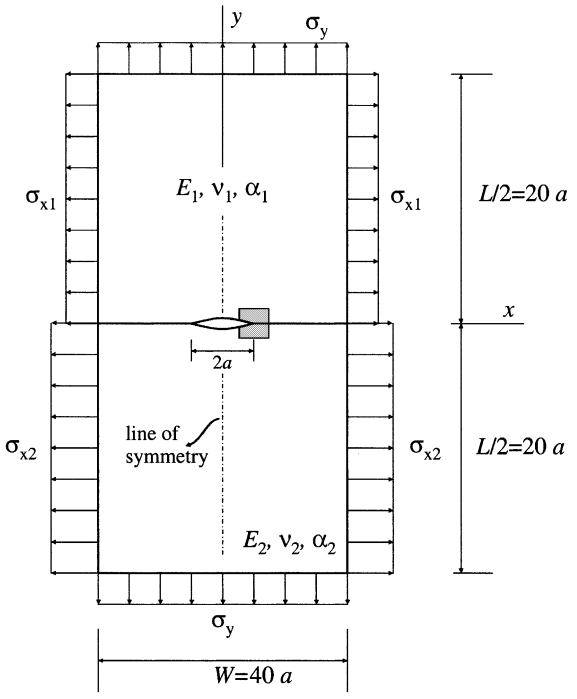

Fig. 8. A central bi-material interface crack in an infinite plate under uniform stress and strain in vertical and horizontal directions, respectively.

Table 3
Normalized stress intensity factors, $K_i^* = K_1/\sigma_0\sqrt{\pi a}$ with $(i = 1, 2)$ for an infinite plate with interface crack by using global elements with 9 and 17 common nodes

E_1/E_2	ν_1/ν_2	Rice and Sih (1965)		Present analysis (9 common nodes)				Present analysis (17 common nodes)			
		K_1^*	K_2^*	K_1^*	K_2^*	Percent difference		K_1^*	K_2^*	Percent difference	
						K_1^*	K_2^*			K_1^*	K_2^*
10	1	1.009	−0.122	1.006	−0.120	0.41	1.73	1.012	−0.123	−0.26	−0.51
22	0.857	1.011	−0.126	1.007	−0.125	0.41	0.48	1.012	−0.127	−0.19	−0.73
100	1	1.014	−0.147	1.011	−0.147	0.31	0.47	1.017	−0.149	−0.26	−0.89

modulus and Poisson's ratio of the second material are varied as shown in Table 3. The center crack length-to-plate width ratio, $2a/W$, is specified as 0.05, with $W = 40$ in. In the direction perpendicular to the interface, the plate is subjected to a uniform stress of $\sigma_0 = 1$ lb/in.^{2}. In order to achieve uniform strain in the direction horizontal to the interface, the first material is subjected to a horizontal stress of $\sigma_{x1} = 0$ and the second material to $\sigma_{x2} = (\nu_2 - \nu_1 E_2/E_1)\sigma_0$. The exact solution for this geometry and loading conditions was reported by Rice and Sih (1965). As presented in Table 3, the comparison of the present analysis results with the exact solution is remarkably favorable. Referring to the inset in Fig. 7, the results presented in Table 3 are obtained with two different global element configurations, i.e., 9 and 17 common

Table 4
Dependency of the normalized stress intensity factors on the global element size and conventional mesh type

h/a	Number of elements	Mesh type	$K_1/\sigma_0\sqrt{\pi a}$	$K_2/\sigma_0\sqrt{\pi a}$	Percent difference	
					K_1	K_2
0.8	20 000	u	1.01246	−0.12343	0.25	0.82
1	12 800	u	1.01224	−0.12345	0.23	0.83
0.2	4920	g	1.01186	−0.12352	0.29	0.79
0.4	2924	g	1.01281	−0.12340	0.27	0.79
0.6	2160	g	1.01265	−0.12339	0.25	0.77
0.8	1674	g	1.01238	−0.12337	0.23	0.80
1	1400	g	1.01226	−0.12340	0.21	0.81
1.2	1242	g	1.01206	−0.12342	0.16	0.75
1.4	1056	g	1.01149	−0.12334	0.15	0.85
1.6	920	g	1.01145	−0.12347	0.10	0.87

Table 5
Dependency of the normalized stress intensity factors, $K_i^* = K_1/\sigma_0\sqrt{\pi a}$ with $(i = 1, 2)$ on the number of eigenvalues (roots) retained in the analysis

Number of eigenvalues	K_1^*	K_2^*	J-Integral	Percent difference	
				K_1^*	K_2^*
25	1.01114	−0.12347	1.64592	0.12	0.85
30	1.01105	−0.12329	1.64555	0.11	0.71
35	1.01099	−0.12333	1.64537	0.11	0.74
40	1.01089	−0.12336	1.64507	0.10	0.77
45	1.01094	−0.12347	1.64529	0.10	0.85

nodes with conventional finite elements. The global element with 9 common nodes had a size of $h_x = 0.4379a$ and $h_y = 0.5009a$ whereas these parameters were $h_x = 0.9065a$ and $h_y = 1.0663a$ for the global element with 17 common nodes.

Considering the same infinite bi-material plate having an interface crack, the effects of the global element size and the number of eigenvalues retained in the series representations in the solution method on the stress intensity factors are investigated. Table 4 presents the stress intensity factors for varying global element size for a specified ratio of Young's moduli and Poisson's ratios, $E_1/E_2 = 10$ and $v_1/v_2 = 1$, respectively. The normalized global element size is defined by $h = h_x = h_y$ as shown in Fig. 7. Also, the effect of the number of conventional finite elements with either a uniform or graded mesh (denoted by u and g in the table) is captured. When all the elements in the finite element model are squares, the mesh is referred to as uniform. If the mesh is refined toward the crack tip, it is referred to as graded. It is observed in Table 4 that the present results differ from the exact solution given by Rice and Sih (1965) by less than 1%. In Table 5, the effect of the number of eigenvalues retained in the series representation on the stress intensity factors is captured by considering 25–45 eigenvalues; the minimum number of eigenvalues required for the current global element is 23. It is apparent that there is no significant dependence on the number of eigenvalues since the percent difference with the exact solution for K_1 and K_2 is always less than 1%.

3.3. Crack perpendicular to interface of bi-material strip

In the case of a crack perpendicular to the interface of dissimilar materials, the stress intensity factors, K_1 and K_2, are calculated and compared with the results reported by Gadi et al. (1995). The geometry of the

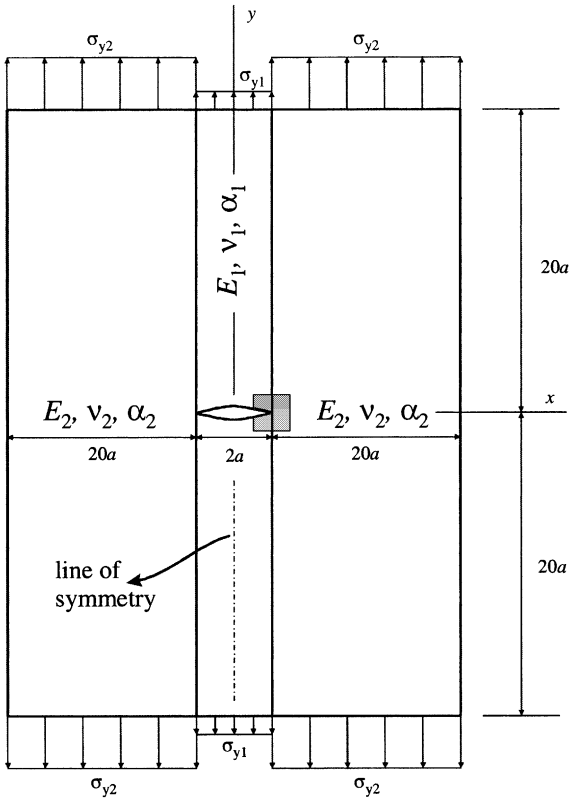

Fig. 9. A crack perpendicular to interface of a bi-material strip under uniform strain.

plate is shown in Fig. 9. The plate is subjected to constant strain, resulting in $\sigma_{y2} = \sigma_{y1}G_2(1-\nu_1)/G_1(1-\nu_2)$. As assigned by Gadi et al., both materials have the same Poisson's ratio, $\nu_1 = \nu_2$, and the ratio of their shear moduli, G_1/G_2, varies from 1 to 10. The center crack length-to-plate width ratio, $2a/W$, is specified as 0.5, with $W = 4$. The length of the strip is specified as $20a$. The results presented in Table 6 are obtained with the conventional finite element model using two different global elements, as in previous cases, one with 9 and the other with 17 common nodes (refer to Fig. 7), having the sizes of $h_x = h_y = h = 0.2195a$ and $h_x = h_y = h = 0.44146a$, respectively. Under plane strain conditions, the stress intensity factors from the present analysis are compared with the values reported by Gadi et al. As presented in Table 6, the comparison of the present analysis results with those available in the literature is favorable.

Table 6
Normalized stress intensity factor, $K_1/\sigma_0\pi a^{\omega_1}$ with $\omega_1 = \mathrm{Re}(\lambda_1)$, for a crack perpendicular to the interface of a bi-material strip by using global elements with 9 and 17 common nodes

E_2/E_1	σ_{y2}/σ_1	$\nu_1 = \nu_2$	Gadi et al. (1995)			Present analysis	
			Gupta	FRAC2D	ABAQUS	9 Common nodes	17 Common nodes
10		0.2	4.922	4.885	4.912	4.942	4.924
10		0.35	3.070	3.079	3.070	3.094	3.076
0.1		0.2	0.699	0.798	0.808	0.795	0.797
0.1		0.35	0.731	0.836	0.844	0.834	0.834

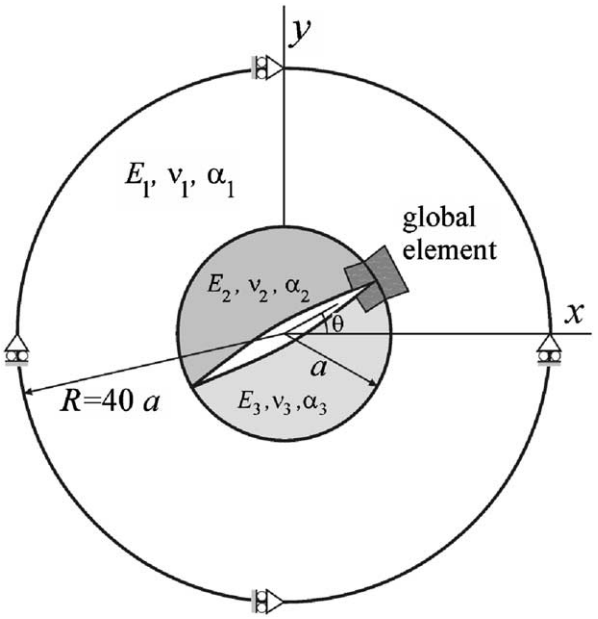

Fig. 10. A circular bi-material inclusion with an interface crack embedded in an infinite plate under thermal loading.

3.4. Circular bi-material inclusion embedded in an infinite plate under thermal loading

Finally, a circular bi-material inclusion embedded in a different material infinite in extent and under a uniform temperature is considered. As shown in Fig. 10, a crack is situated between the two semi-circular inclusions with an inclination angle of θ. The material properties and geometric parameters are specified by $R/a = 40$, with $a = 1$ in.; $E_2/E_1 = 10$, $E_3/E_1 = 25$; $\nu_1 = \nu_2 = \nu_3 = 0.3$; $\alpha_1/\alpha_2 = 2$; and $\alpha_1/\alpha_3 = 20$. For an applied uniform temperature change of $\alpha_3 \Delta T = 100$, the normalized stress intensity factors are calculated as $K_1/(\alpha_3 \Delta T E_1 a^{\omega_1}) = 0.081019$ and $K_2/(\alpha_3 \Delta T E_1 a^{\omega_1}) = -0.155642$ with ω_1 representing the real part of λ_1. Because of the axisymmetric nature of the loading and geometry, the stress intensity factors are independent of the crack inclination angle.

4. Conclusions

In order to capture the singular stress field under mechanical and thermal loading in the regions addressing either an open or a closed junction of multiple dissimilar materials, a hybrid global (special) element has been developed utilizing the exact solution for the stress and displacement fields based on the eigenfunction expansion method. The global element for arbitrary geometrical and material configurations is coupled with traditional (local) elements while satisfying the inter-element continuity. The coupling between the hybrid global element and conventional finite elements is implemented into ANSYS, a commercially available finite element program. Also, the global element is integrated into the ANSYS graphical user interface for pre- and post-processing. The solution method is validated through existing asymptotic solutions and conventional detailed finite element analysis.

Appendix A

The non-dimensional functions $F^{(k)}_{\alpha\beta}(\theta;\lambda_n)$, $G^{(k)}_{\alpha}(\theta;\lambda_n)$, $f^{(k)}_{\alpha\beta}(\theta)$, $g^{(k)}_{\alpha}(\theta)$ and $h^{(k)}_{\alpha}(\theta)$ in Eqs. (1) and (2) can be derived as

$$F^{(k)}_{rr}(\theta;\lambda_n)=\frac{(2-\lambda_n)}{4}\left[A^{(k)}_n\cos\lambda_n\theta+B^{(k)}_n\sin\lambda_n\theta\right]-\left[C^{(k)}_n\cos(\lambda_n+2)\theta+D^{(k)}_n\sin(\lambda_n+2)\theta\right] \tag{A.1}$$

$$F^{(k)}_{\theta\theta}(\theta;\lambda_n)=\frac{(2+\lambda_n)}{4}\left[A^{(k)}_n\cos\lambda_n\theta+B^{(k)}_n\sin\lambda_n\theta\right]+\left[C^{(k)}_n\cos(\lambda_n+2)\theta+D^{(k)}_n\sin(\lambda_n+2)\theta\right] \tag{A.2}$$

$$F^{(k)}_{r\theta}(\theta;\lambda_n)=\frac{\lambda_n}{4}\left[A^{(k)}_n\sin\lambda_n\theta-B^{(k)}_n\cos\lambda_n\theta\right]+\left[C^{(k)}_n\sin(\lambda_n+2)\theta-D^{(k)}_n\cos(\lambda_n+2)\theta\right] \tag{A.3}$$

$$G^{(k)}_r=\left\{\frac{(2-\lambda_n)-\nu_k(2+\lambda_n)}{4E_k(\lambda_n+1)}\left[A^{(k)}_n\cos\lambda_n\theta+B^{(k)}_n\sin\lambda_n\theta\right]-\frac{1+\nu_k}{E_k(\lambda_n+1)}\left[C^{(k)}_n\cos(\lambda_n+2)\theta+D^{(k)}_n\sin(\lambda_n+2)\theta\right]\right\} \tag{A.4}$$

$$G^{(k)}_\theta=\left\{\frac{\lambda_n(1+\nu_k)+4}{4E_k(\lambda_n+1)}\left[A^{(k)}_n\sin\lambda_n\theta+B^{(k)}_n\cos\lambda_n\theta\right]+\frac{1+\nu_k}{E_k(\lambda_n+1)}\left[C^{(k)}_n\sin(\lambda_n+2)\theta-D^{(k)}_n\cos(\lambda_n+2)\theta\right]\right\} \tag{A.5}$$

$$f^{(k)}_{rr}(\theta)=A^{(k)}_c\cos2\theta+B^{(k)}_c\sin2\theta+\tfrac{1}{2}C^{(k)}_c\theta+\tfrac{1}{2}D^{(k)}_c \tag{A.6}$$

$$f^{(k)}_{\theta\theta}(\theta)=-A^{(k)}_c\cos2\theta-B^{(k)}_c\sin2\theta+\tfrac{1}{2}C^{(k)}_c\theta+\tfrac{1}{2}D^{(k)}_c \tag{A.7}$$

$$f^{(k)}_{r\theta}(\theta)=B^{(k)}_c\cos2\theta-A^{(k)}_c\sin2\theta-\tfrac{1}{4}C^{(k)}_c \tag{A.8}$$

$$g^{(k)}_r(\theta)=\frac{(1+\nu_k)}{E_k}\left[A^{(k)}_c\cos2\theta+B^{(k)}_c\sin2\theta\right]+\frac{(1-\nu_k)}{2E_k}\left[C^{(k)}_c\theta+\frac{1}{2}D^{(k)}_c\right] \tag{A.9}$$

$$g^{(k)}_\theta(\theta)=-\frac{(1+\nu_k)}{E_k}\left[A^{(k)}_c\sin2\theta-B^{(k)}_c\cos2\theta\right]+E^{(k)}_c \tag{A.10}$$

$$h^{(k)}_r(\theta)=0;\quad h^{(k)}_\theta(\theta)=-\frac{1}{E_k}C^{(k)}_c \tag{A.11}$$

in which $A^{(k)}_n$, $B^{(k)}_n$, $C^{(k)}_n$, $D^{(k)}_n$, $A^{(k)}_c$, $B^{(k)}_c$, $C^{(k)}_c$, $D^{(k)}_c$, and $E^{(k)}_c$ are the unknown coefficients associated with the kth sector.

The matrices $\mathbf{P}_c^{(k)}$, $\mathbf{P}_n^{(k)}$, $\mathbf{T}_c^{(k)}$, and $\mathbf{T}_n^{(k)}$ in Eqs. (3)–(6) are given by

$$\mathbf{P}_c^{(k)}(\theta) = \begin{bmatrix} -\cos 2\theta & -\sin 2\theta & \frac{\theta}{2} & \frac{1}{2} & 0 \\ -\sin 2\theta & \cos 2\theta & -\frac{1}{4} & 0 & 0 \\ \frac{1+\nu_k}{E_k}\cos 2\theta & \frac{1+\nu_k}{E_k}\sin\theta & \frac{1-\nu_k}{2E_k}\theta & \frac{1-\nu_k}{2E_k} & 0 \\ -\frac{1+\nu_k}{E_k}\sin 2\theta & \frac{1+\nu_k}{E_k}\cos 2\theta & 0 & 0 & 1 \\ 0 & 0 & -\frac{1}{E_k} & 0 & 0 \end{bmatrix} \tag{A.12}$$

$$\mathbf{P}_n^{(k)}(\theta;\lambda_n) = \begin{bmatrix} \frac{2+\lambda_n}{4}\cos\lambda_n\theta & \frac{2+\lambda_n}{4}\sin\lambda_n\theta & \cos(\lambda+2)\theta & \sin(\lambda_n+2)\theta \\ \frac{\lambda_n}{4}\sin\lambda_n\theta & -\frac{\lambda_n}{4}\cos\lambda_n\theta & \sin(\lambda+2)\theta & -\cos(\lambda_n+2)\theta \\ \frac{(2-\lambda_n)-\nu_k(2+\lambda_n)}{4E_k(1+\lambda_n)}\cos\lambda_n\theta & \frac{(2-\lambda_n)-\nu_k(2+\lambda_n)}{4E_k(1+\lambda_n)}\sin\lambda_n\theta & -\frac{1+\nu_k}{E_k(1+\lambda_n)}\cos(\lambda_n+2)\theta & -\frac{1+\nu_k}{E_k(1+\lambda_n)}\sin(\lambda_n+2)\theta \\ \frac{\lambda_n(1+\nu_k)+4}{4E_k(1+\lambda_n)}\sin\lambda_n\theta & -\frac{\lambda_n(1+\nu_k)+4}{4E_k(1+\lambda_n)}\cos\lambda_n\theta & \frac{1+\nu_k}{E_k(1+\lambda_n)}\sin(\lambda_n+2)\theta & -\frac{1+\nu_k}{E_k(1+\lambda_n)}\cos(\lambda_n+2)\theta \end{bmatrix} \tag{A.13}$$

$$\mathbf{T}_c^{(k)}(\theta) = \begin{bmatrix} -\cos 2\theta & -\sin 2\theta & \frac{\theta}{2} & \frac{1}{2} & 0 \\ -\sin 2\theta & \cos 2\theta & -\frac{1}{4} & 0 & 0 \end{bmatrix} \tag{A.14}$$

$$\mathbf{T}_n^{(k)}(\theta;\lambda_n) = \begin{bmatrix} \frac{2+\lambda_n}{4}\cos\lambda_n\theta & \frac{2+\lambda_n}{4}\sin\lambda_n\theta & \cos(\lambda_n+2)\theta & \sin(\lambda_n+2)\theta \\ \frac{\lambda_n}{4}\sin\lambda_n\theta & -\frac{\lambda_n}{4}\cos\lambda_n\theta & \sin(\lambda_n+2)\theta & -\cos(\lambda_n+2)\theta \end{bmatrix} \tag{A.15}$$

The expression for the rotation of the first material sector, which results in the constraint condition of no rigid-body rotation is given in the form

$$\omega^{(1)} = \frac{\nu_1 - 3}{4E_1}C_c^{(1)} + E_c^{(1)} - \frac{4}{E_1}\ln r C_c^{(1)} + \sum_{n=1}^{\infty} r^{\lambda_n}\frac{1}{E_1}\left[A_c^{(1)}\sin\lambda_n\theta - B_c^{(1)}\sin\lambda_n\theta\right] \tag{A.16}$$

obtained form

$$\omega^{(1)} = \frac{1}{2r}\left[\frac{\partial(r u_\theta^{(1)})}{\partial r} - \frac{\partial u_r^{(1)}}{\partial\theta}\right] \tag{A.17}$$

The known vectors, $\mathbf{r}_j$, with $j = \mathrm{C}, \mathrm{O}$, in Eq. (23) are defined as

$$\mathbf{r}_{\mathrm{O}}^T = \left\{\mathbf{0}^T, \mathbf{r}_c^{(1)^T} - \mathbf{r}_c^{(2)^T}, \mathbf{r}_c^{(2)^T} - \mathbf{r}_c^{(3)^T}, \ldots, \mathbf{r}_c^{(K-1)^T} - \mathbf{r}_c^{(K)^T}, \mathbf{0}^T, 0\right\} \tag{A.18}$$

and

$$\mathbf{r}_{\mathrm{C}}^T = \left\{{}^*\mathbf{r}_c^{(1)^T} - {}^*\mathbf{r}_c^{(K)^T}, \mathbf{r}_c^{(1)^T} - \mathbf{r}_c^{(2)^T}, \mathbf{r}_c^{(2)^T} - \mathbf{r}_c^{(3)^T}, \ldots, \mathbf{r}_c^{(K-1)^T} - \mathbf{r}_c^{(K)^T}, 0\right\} \tag{A.19}$$

in which the vector ${}^*\mathbf{r}_c^{(k)}$ is a modified form of $\mathbf{r}_c^{(k)}$ defined as

$${}^*\mathbf{r}_c^{(k)^T} = \{0, 0, -\kappa_k T_0, 0\} \tag{A.20}$$

The coefficient matrices, $\mathbf{S}_j$ $(j = \mathrm{C}, \mathrm{O})$, in Eq. (23) are associated with the non-homogeneous system of equations and defined as

$$\mathbf{S}_{\mathrm{O}} = \begin{bmatrix} \mathbf{T}_c^{(1)}(0) & 0 & 0 & \cdots & 0 \\ \mathbf{P}_c^{(1)}(\theta_1) & -\mathbf{P}_c^{(2)}(\theta_1) & 0 & \cdots & 0 \\ 0 & \mathbf{P}_c^{(2)}(\theta_2) & -\mathbf{P}_c^{(3)}(\theta_2) & \cdots & 0 \\ \vdots & \vdots & & & \vdots \\ \vdots & \vdots & & \mathbf{P}_c^{(K-1)}(\theta_{K-1}) & -\mathbf{P}_c^{(K)}(\theta_{K-1}) \\ 0 & 0 & \mathbf{0} & \mathbf{0} & \mathbf{T}_c^{(K)}(\theta_K) \\ \mathbf{C}_R & 0 & 0 & 0 & 0 \end{bmatrix} \tag{A.21}$$

and

$$\mathbf{S}_{\mathrm{C}} = \begin{bmatrix} {}^*\mathbf{P}_c^{(1)}(0) & 0 & 0 & \cdots & -{}^*\mathbf{P}_c^{(K)}(2\pi) \\ \mathbf{P}_c^{(1)}(\theta_1) & -\mathbf{P}_c^{(2)}(\theta_1) & 0 & \cdots & 0 \\ 0 & \mathbf{P}_c^{(2)}(\theta_2) & -\mathbf{P}_c^{(3)}(\theta_2) & \cdots & 0 \\ \vdots & \vdots & & & \vdots \\ \vdots & \vdots & & & \vdots \\ 0 & 0 & 0 & \mathbf{P}_c^{(K-1)}(\theta_{K-1}) & -\mathbf{P}_c^{(K)}(\theta_{K-1}) \\ \mathbf{C}_R & 0 & 0 & 0 & 0 \end{bmatrix} \tag{A.22}$$

in which ${}^*\mathbf{P}_c^{(k)}$ $(k = 1, K)$ is a modified form of $\mathbf{P}_c^{(k)}$defined as

$${}^*\mathbf{P}_c^{(k)}(\theta) = \begin{bmatrix} -\cos 2\theta & -\sin 2\theta & \frac{\theta}{2} & \frac{1}{2} & 0 \\ -\sin 2\theta & \cos 2\theta & -\frac{1}{4} & 0 & 0 \\ \frac{1+\nu_k}{E_k}\cos 2\theta & \frac{1+\nu_k}{E_k}\sin\theta & \frac{1-\nu_k}{2E_k}\theta & \frac{1-\nu_k}{2E_k} & 0 \\ -\frac{1+\nu_k}{E_k}\sin 2\theta & \frac{1+\nu_k}{E_k}\cos 2\theta & 0 & 0 & 1 \end{bmatrix} \tag{A.23}$$

The modification of $\mathbf{r}_c^{(k)}$ and $\mathbf{P}_c^{(k)}$ as ${}^*\mathbf{r}_c^{(k)}$ and ${}^*\mathbf{P}_c^{(k)}$ removes the redundant equation arising from

$$h_\theta^{(1)}(0) - h_\theta^{(K)}(2\pi) = 0 \tag{A.24}$$

in the case of a closed junction, leading to

$$-\frac{1}{E_1}C_c^{(1)} + \frac{1}{E_k}C_c^{(K)} = 0 \tag{A.25}$$

The coefficient matrices, $\mathbf{Q}_j(\lambda_n)$, with $(j = \mathrm{C}, \mathrm{O})$, in Eq. (23) are associated with the homogeneous system of equations and defined by

$$\mathbf{Q}_{\mathrm{C}} = \begin{bmatrix} \mathbf{P}_n^{(1)}(0;\lambda_n) & 0 & 0 & \cdots & -\mathbf{P}_n^{(K)}(2\pi;\lambda_n) \\ \mathbf{P}_n^{(1)}(\theta_1;\lambda_n) & -\mathbf{P}_n^{(2)}(\theta_1;\lambda_n) & 0 & \cdots & 0 \\ 0 & \mathbf{P}_n^{(2)}(\theta_2;\lambda_n) & -\mathbf{P}_n^{(3)}(\theta_2;\lambda_n) & \cdots & 0 \\ \vdots & \vdots & & & \vdots \\ \vdots & \vdots & & & \vdots \\ 0 & 0 & 0 & \mathbf{P}_n^{(K-1)}(\theta_{K-1};\lambda_n) & \mathbf{P}_n^{(K)}(\theta_{K-1};\lambda_n) \end{bmatrix} \tag{A.26}$$

and

$$\mathbf{Q}_{\mathrm{O}} = \begin{bmatrix} \mathbf{T}_n^{(1)}(0;\lambda_n) & 0 & 0 & \cdots & 0 \\ \mathbf{P}_n^{(1)}(\theta_1;\lambda_n) & -\mathbf{P}_n^{(2)}(\theta_1;\lambda_n) & 0 & \cdots & 0 \\ 0 & \mathbf{P}_n^{(2)}(\theta_2;\lambda_n) & -\mathbf{P}_n^{(3)}(\theta_2;\lambda_n) & \cdots & 0 \\ \vdots & \vdots & & & \vdots \\ \vdots & \vdots & & \mathbf{P}_n^{(K-1)}(\theta_{K-1};\lambda_n) & \mathbf{P}_n^{(K)}(\theta_{K-1};\lambda_n) \\ 0 & 0 & \mathbf{0} & \mathbf{0} & \mathbf{T}_n^{(K)}(\theta_K;\lambda_n) \end{bmatrix} \tag{A.27}$$

Appendix B

The total potential in the domain of multiple dissimilar material sectors under only thermal loading can be expressed as

$$\pi = \sum_{k=1}^{K} \left\{ \frac{1}{2} \int_{A_k} C_{\alpha\beta\gamma\eta}^{(k)}\, {}^{t}\varepsilon_{\alpha\beta}^{(k)}\, {}^{t}\varepsilon_{\gamma\eta}^{(k)}\, \mathrm{d}A - \int_{A_k} C_{\alpha\beta\gamma\eta}^{(k)}\, {}^{\circ}\varepsilon_{\alpha\beta}^{(k)}\, {}^{t}\varepsilon_{\gamma\eta}^{(k)}\, \mathrm{d}A - \int_{\hat{\Gamma}_k} {}^{t}\hat{t}_{\alpha}^{(k)} ({}^{t}u_{\alpha}^{(k)} - {}^{t}\hat{u}_{\alpha}^{k})\, \mathrm{d}\Gamma \right\} \tag{B.1}$$

with $\alpha, \beta, \gamma, \eta = x, y$. The strain components, ${}^{t}\varepsilon_{\alpha\beta}^{(k)}$, arise from the uniform temperature variation, T_0. Its non-stress-producing strain components in each material sector are denoted by ${}^{\circ}\varepsilon_{\alpha\beta}^{(k)}$ and defined as

$${}^{\circ}\varepsilon_{\alpha\beta}^{(k)} = \kappa^{(k)} T_0 \delta_{\alpha\beta} \tag{B.2}$$

The displacement components are denoted by ${}^{t}u_{\alpha}^{(k)}$. Requiring the first variation of the total potential to vanish results in

$$\begin{aligned} \delta\pi &= \sum_{k=1}^{K} \left\{ \int_{A_k} C_{\alpha\beta\gamma\eta}^{(k)} ({}^{t}\varepsilon_{\alpha\beta}^{(k)} - {}^{\circ}\varepsilon_{\alpha\beta}^{(k)}) \delta {}^{t}\varepsilon_{\gamma\eta}^{(k)}\, \mathrm{d}A \right\} - \sum_{k=1}^{K} \left\{ \int_{\hat{\Gamma}_k} \delta {}^{t}\hat{t}_{\alpha}^{(k)} ({}^{t}u_{\alpha}^{(k)} - {}^{t}\hat{u}_{\alpha}^{k})\, \mathrm{d}\Gamma + \int_{\hat{\Gamma}_k} {}^{t}\hat{t}_{\alpha}^{(k)} \delta ({}^{t}u_{\alpha}^{(k)} - {}^{t}\hat{u}_{\alpha}^{k})\, \mathrm{d}\Gamma \right\} \\ &= 0 \end{aligned} \tag{B.3}$$

The stress components due to the thermal loading are expressed as

$${}^{t}\sigma_{\alpha\beta}^{(k)} = C_{\alpha\beta\gamma\eta}^{(k)} ({}^{t}\varepsilon_{\gamma\eta}^{(k)} - {}^{\circ}\varepsilon_{\gamma\eta}^{(k)}) \tag{B.4}$$

in which the material property tensor $C_{\alpha\beta\gamma\eta}^{(k)}$ for each sector is specified by

$$C^{(k)}_{\alpha\beta\gamma\eta} = \frac{E_k}{(1+\nu_k)}\delta_{\gamma\alpha}\delta_{\beta\eta} + \frac{\nu_k E_k}{(1+\nu_k)(1-2\nu_k)}\delta_{\alpha\beta}\delta_{\gamma\eta} \tag{B.5}$$

The unknown components of the traction vector along the common boundary segments, $\hat{\Gamma}_k$, shown in Fig. 2, are denoted by ${}^t\hat{t}^k_\alpha$ and ${}^t\hat{u}^k_\alpha$ with

$${}^t\hat{t}^{(k)}_\alpha = {}^t\sigma^{(k)}_{\alpha\beta}\hat{n}^{(k)}_\beta \tag{B.6}$$

Substituting for the thermal strain components from Eq. (B.6) along with the strain–displacement relations in the expression for the total potential results in

$$\delta\pi = \sum_{k=1}^{K}\left\{\int_{A_k} {}^t\sigma^{(k)}_{\alpha\beta}\delta^t u^{(k)}_{\alpha,\beta}\,\mathrm{d}A\right\} - \sum_{k=1}^{K}\left\{\int_{\hat{\Gamma}_k}\delta^t\hat{t}^{(k)}_\alpha({}^t u^{(k)}_\alpha - {}^t\hat{u}^{(k)}_\alpha)\,\mathrm{d}\Gamma + \int_{\hat{\Gamma}_k}{}^t\hat{t}^{(k)}_\alpha\delta({}^t u^{(k)}_\alpha - {}^t\hat{u}^{(k)}_\alpha)\,\mathrm{d}\Gamma\right\} = 0 \tag{B.7}$$

Applying the divergence theorem leads to

$$\begin{aligned}\delta\pi = \sum_{k=1}^{K}\Bigg\{ &-\int_{A_k}{}^t\sigma^{(k)}_{\alpha\beta,\beta}\delta^t u^{(k)}_\alpha\,\mathrm{d}A + \int_{\Gamma_k}{}^t\sigma^{(k)}_{\alpha\beta}n^{(k)}_\beta\delta^t u^{(k)}_\alpha\,\mathrm{d}\Gamma\Bigg\} - \sum_{k=1}^{K}\Bigg\{\int_{\hat{\Gamma}_k}\delta^t\hat{t}^{(k)}_\alpha({}^t u^{(k)}_\alpha - {}^t\hat{u}^{(k)}_\alpha)\,\mathrm{d}\Gamma \\ &+ \int_{\hat{\Gamma}_k}{}^t\hat{t}^{(k)}_\alpha\delta({}^t u^{(k)}_\alpha - {}^t\hat{u}^{(k)}_\alpha)\,\mathrm{d}\Gamma\Bigg\} = 0\end{aligned} \tag{B.8}$$

The first boundary integral describing each sector Γ_k can be decomposed as

$$\begin{aligned}\sum_{k=1}^{K}\int_{\Gamma_k}{}^t\sigma^{(k)}_{\alpha\beta}n^{(k)}_\beta\delta^t u^{(k)}_\alpha\,\mathrm{d}\Gamma = &\sum_{k=1}^{K-1}\int_{\bar{\Gamma}_k}{}^t\sigma^{(k)}_{\alpha\beta}\tilde{n}^{(k)}_\beta\delta^t u^{(k)}_\alpha\,\mathrm{d}\Gamma + \int_{\overline{\Gamma}_K}{}^t\sigma^{(K)}_{\alpha\beta}\tilde{n}^{(K)}_\beta\delta^t u^{(K)}_\alpha\,\mathrm{d}\Gamma \\ &+ \sum_{k=2}^{K}\int_{\overline{\Gamma}_k}{}^t\sigma^{(k)}_{\alpha\beta}\bar{n}^{(k)}_\beta\delta^t u^{(k)}_\alpha\,\mathrm{d}\Gamma + \int_{\overline{\Gamma}_1}{}^t\sigma^{(1)}_{\alpha\beta}\bar{n}^{(1)}_\beta\delta^t u^{(1)}_\alpha\,\mathrm{d}\Gamma \\ &+ \sum_{k=1}^{K}\int_{\hat{\Gamma}_k}{}^t\sigma^{(k)}_{\alpha\beta}\hat{n}^{(k)}_\beta\delta^t u^{(k)}_\alpha\,\mathrm{d}\Gamma\end{aligned} \tag{B.9}$$

or

$$\begin{aligned}\sum_{k=1}^{K}\int_{\Gamma_k}{}^t\sigma^{(k)}_{\alpha\beta}n^{(k)}_\beta\delta^t u^{(k)}_\alpha\,\mathrm{d}\Gamma = &\sum_{k=1}^{K-1}\left\{\int_{\bar{\Gamma}_k}{}^t\sigma^{(k)}_{\alpha\beta}\tilde{n}^{(k)}_\beta\delta^t u^{(k)}_\alpha\,\mathrm{d}\Gamma + \int_{\overline{\Gamma}_{k+1}}{}^t\sigma^{(k+1)}_{\alpha\beta}\bar{n}^{(k+1)}_\beta\delta^t u^{(k+1)}_\alpha\,\mathrm{d}\Gamma\right\} \\ &+ \int_{\bar{\Gamma}_K}{}^t\sigma^{(K)}_{\alpha\beta}\tilde{n}^{(K)}_\beta\delta^t u^{(K)}_\alpha\,\mathrm{d}\Gamma + \int_{\overline{\Gamma}_1}{}^t\sigma^{(1)}_{\alpha\beta}\bar{n}^{(1)}_\beta\delta^t u^{(1)}_\alpha\,\mathrm{d}\Gamma \\ &+ \sum_{k=1}^{K}\int_{\hat{\Gamma}_k}{}^t\sigma^{(k)}_{\alpha\beta}\hat{n}^{(k)}_\beta\delta^t u^{(k)}_\alpha\,\mathrm{d}\Gamma\end{aligned} \tag{B.10}$$

The continuity conditions between the adjacent sectors require that

$${}^t\tilde{u}^{(k)}_\alpha = {}^t\bar{u}^{(k+1)}_\alpha \tag{B.11}$$

$${}^t\sigma^{(k)}_{\alpha\beta}\tilde{n}^{(k)}_\alpha = -{}^t\sigma^{(k+1)}_{\alpha\beta}\bar{n}^{(k+1)}_\alpha \tag{B.12}$$

with $k = 1,\ldots,K-1$. For a closed junction, the additional continuity conditions are

$$ {}^{t}\tilde{u}_{\alpha}^{(K)} = {}^{t}\bar{u}_{\alpha}^{(1)} \tag{B.13} $$

$$ {}^{t}\sigma_{\alpha\beta}^{(K)}\tilde{n}_{\alpha}^{(K)} = -{}^{t}\sigma_{\alpha\beta}^{(1)}\bar{n}_{\alpha}^{(1)} \tag{B.14} $$

In the presence of an open junction with traction-free surfaces, the additional continuity equations are replaced by

$$ {}^{t}\sigma_{\alpha\beta}^{(K)}\tilde{n}_{\alpha}^{(K)} = {}^{t}\sigma_{\alpha\beta}^{(1)}\bar{n}_{\alpha}^{(1)} = 0 \tag{B.15} $$

Enforcing these conditions and noting that the adjacent boundaries are related to each other by $\widetilde{\Gamma}_k = \overline{\Gamma}_{k+1}$ and $\widetilde{\Gamma}_K = \overline{\Gamma}_1$ for a closed junction, Eq. (B.13) is reduced to

$$ \sum_{k=1}^{K}\int_{\Gamma_k} {}^{t}\sigma_{\alpha\beta}^{(k)} n_{\beta}^{(k)}\delta^{t}u_{\alpha}^{(k)}\,\mathrm{d}\Gamma = \sum_{k=1}^{K}\int_{\hat{\Gamma}_k} {}^{t}\sigma_{\alpha\beta}^{(k)}\hat{n}_{\beta}^{(k)}\delta^{t}u_{\alpha}^{(k)}\,\mathrm{d}\Gamma \tag{B.16} $$

With this substitution, the final form of the first variation of the total potential becomes

$$ \begin{aligned} \delta\pi = \sum_{k=1}^{K}\Bigg\{ &-\int_{A_k} {}^{t}\sigma_{\alpha\beta,\beta}^{(k)}\delta^{t}u_{\alpha}^{(k)}\,\mathrm{d}A + \int_{\hat{\Gamma}_k} {}^{t}\sigma_{\alpha\beta}^{(k)}\hat{n}_{\beta}^{(k)}\delta^{t}u_{\alpha}^{(k)}\,\mathrm{d}\Gamma\Bigg\} - \sum_{k=1}^{K}\Bigg\{\int_{\hat{\Gamma}_k}\delta^{t}\hat{t}_{\alpha}^{(k)}({}^{t}u_{\alpha}^{(k)} - {}^{t}\hat{u}_{\alpha}^{(k)})\,\mathrm{d}\Gamma \\ &+ \int_{\hat{\Gamma}_k} {}^{t}\hat{t}_{\alpha}^{(k)}\delta({}^{t}u_{\alpha}^{(k)} - {}^{t}\hat{u}_{\alpha}^{(k)})\,\mathrm{d}\Gamma\Bigg\} = 0 \end{aligned} \tag{B.17} $$

leading to the governing equations

$$ {}^{t}\sigma_{\alpha\beta,\beta}^{(k)} = 0 \quad \text{in } A_k \tag{B.18} $$

$$ {}^{t}\hat{t}_{\alpha}^{(k)} = {}^{t}\sigma_{\alpha\beta}^{(k)}\hat{n}_{\beta}^{(k)} \quad \text{on } \hat{\Gamma}_k \tag{B.19} $$

$$ {}^{t}\hat{t}_{\alpha}^{(k)} = 0 \quad \text{on } \hat{\Gamma}_k \tag{B.20} $$

$$ {}^{t}u_{\alpha}^{(k)} = \hat{u}_{\alpha}^{(k)} \text{ on } \hat{\Gamma}_k \tag{B.21} $$

The expressions for the stress components given in Eqs. (36) and (37) automatically satisfy the equilibrium equations given by Eq. (B.18). However, it is not guaranteed that these stress components satisfy the condition of zero boundary traction,

$$ {}^{t}\hat{t}_{\alpha}^{(k)} = {}^{t}\sigma_{\alpha\beta}^{(k)}\hat{n}_{\beta}^{(k)} = 0 \quad \text{on } \hat{\Gamma}_k \tag{B.22} $$

Assuming the boundary traction field, ${}^{t}\hat{t}_{\alpha}^{(k)}$, to be zero reduces the first variation of the total potential to

$$ \delta\pi = \sum_{k=1}^{K}\Bigg\{\int_{\hat{\Gamma}_k} {}^{t}\sigma_{\alpha\beta}^{(k)}\hat{n}_{\beta}^{(k)}\delta^{t}u_{\alpha}^{(k)}\,\mathrm{d}\Gamma\Bigg\} = 0 \tag{B.23} $$

This equation leads to the imposition of the condition given by Eq. (B.15) in an average sense through the minimization of the total potential. It is worth noting that this expression is independent of the boundary values; therefore, it can be directly utilized to determine the stress and strain fields arising from thermal

loading. These fields can be treated as known initial quantities in the solution of the same problem under combined mechanical and thermal loadings.

Utilizing the matrix representation of ${}^t\sigma_{\alpha\beta}^{(k)}$ and ${}^t u_\alpha^{(k)}$ in polar coordinates from Eq. (33), the variation of the total potential energy under thermal loading is rewritten as

$$\delta\pi = \sum_{k=1}^{K}\left\{ \int_{\hat{\Gamma}_k} {}^t\boldsymbol{\sigma}_p^{(k)^T}\mathbf{Z}_\sigma^{(k)^T}\hat{\mathbf{n}}^{(k)}\mathbf{Z}_u^{(k)}\delta^t\mathbf{u}_p^{(k)}\,\mathrm{d}\Gamma\right\} = 0 \tag{B.24}$$

where

$${}^t\boldsymbol{\sigma}_p^{(k)} = {}_\lambda{}^t\boldsymbol{\sigma}_p^{(k)} + {}_c{}^t\boldsymbol{\sigma}_p^{(k)} \quad \text{and} \quad {}^t\mathbf{u}_p^{(k)} = {}_\lambda{}^t\mathbf{u}_p^{(k)} + {}_c{}^t\mathbf{u}_p^{(k)} \tag{B.25}$$

The terms ${}_\lambda{}^t\boldsymbol{\sigma}_p^{(k)}$ and ${}_\lambda{}^t\mathbf{u}_p^{(k)}$ are associated with the homogeneous solution of thermal loading. The terms ${}_c{}^t\boldsymbol{\sigma}_p^{(k)}$ and ${}_c{}^t\mathbf{u}_p^{(k)}$ represent the complementary non-singular solution for uniform thermal loading. Therefore, the variation of the displacement field becomes

$$\delta^t\mathbf{u}_p^{(k)} = \delta_\lambda^t\mathbf{u}_p^{(k)} + \delta_c^t\mathbf{u}_p^{(k)} = \delta_\lambda^t\mathbf{u}_p^{(k)} \tag{B.26}$$

Substituting for ${}^t\boldsymbol{\sigma}_p^{(k)}$ and ${}^t\mathbf{u}_p^{(k)}$ results in

$$\delta\pi = \sum_{k=1}^{K}\left\{ \int_{\hat{\Gamma}_k} {}_\lambda{}^t\boldsymbol{\sigma}_p^{(k)^T}\mathbf{Z}_\sigma^{(k)^T}\hat{\mathbf{n}}^{(k)}\mathbf{Z}_u^{(k)}\delta_\lambda^t\mathbf{u}_p^{(k)}\,\mathrm{d}\Gamma + \int_{\hat{\Gamma}_k} {}_c{}^t\boldsymbol{\sigma}_p^{(k)^T}\mathbf{Z}_\sigma^{(k)^T}\hat{\mathbf{n}}^{(k)}\mathbf{Z}_u^{(k)}\delta_\lambda^t\mathbf{u}_p^{(k)}\,\mathrm{d}\Gamma\right\} = 0 \tag{B.27}$$

After substituting for ${}^t\boldsymbol{\sigma}_p^{(k)}$ and ${}^t\mathbf{u}_p^{(k)}$ from Eqs. (36) and (37), this expression can be rewritten as

$$\delta\pi = \sum_{k=1}^{K}\sum_{i=0}^{N}\sum_{j=0}^{N} {}^t\hat{\boldsymbol{\alpha}}_i^T\left\{ \int_{\hat{\Gamma}_k} \hat{\mathbf{F}}_i^{(k)^T}\mathbf{Z}_\sigma^{(k)^T}\hat{\mathbf{n}}^{(k)}\mathbf{Z}_u^{(k)}\hat{\mathbf{G}}_j^{(k)}\,\mathrm{d}\Gamma\right\}\delta^t\hat{\boldsymbol{\alpha}}_j + \sum_{k=1}^{K}\sum_{i=0}^{N}\left\{ \int_{\hat{\Gamma}_k} \mathbf{F}_c^{(k)^T}\mathbf{Z}_\sigma^{(k)^T}\hat{\mathbf{n}}^{(k)}\mathbf{Z}_u^{(k)}\hat{\mathbf{G}}_i^{(k)}\,\mathrm{d}\Gamma\right\}\delta^t\hat{\boldsymbol{\alpha}}_i = 0 \tag{B.28}$$

The transpose of this equation yields

$$\delta\pi = \sum_{k=1}^{K}\sum_{i=0}^{N}\sum_{j=0}^{N}\delta^t\hat{\boldsymbol{\alpha}}_i^T\left\{ \int_{\hat{\Gamma}_k} \hat{\mathbf{G}}_i^{(k)^T}\mathbf{Z}_u^{(k)^T}\hat{\mathbf{n}}^{(k)}\mathbf{Z}_\sigma^{(k)}\hat{\mathbf{F}}_j^{(k)}\,\mathrm{d}\Gamma\right\}{}^t\hat{\boldsymbol{\alpha}}_j + \sum_{k=1}^{K}\sum_{i=0}^{N}\delta^t\hat{\boldsymbol{\alpha}}_i^T\left\{ \int_{\hat{\Gamma}_k} \hat{\mathbf{G}}_i^{(k)^T}\mathbf{Z}_u^{(k)^T}\hat{\mathbf{n}}^{(k)}\mathbf{Z}_\sigma^{(k)}\mathbf{F}_c^{(k)}\,\mathrm{d}\Gamma\right\} = 0 \tag{B.29}$$

This expression can be written in compact form as

$$\delta\pi = \sum_{k=1}^{K}\sum_{i=0}^{N}\sum_{j=0}^{N}\delta^t\hat{\boldsymbol{\alpha}}_i^T\mathbf{H}_{ij}^{(k)}{}^t\hat{\boldsymbol{\alpha}}_j + \sum_{k=1}^{K}\sum_{i=0}^{N}\delta^t\hat{\boldsymbol{\alpha}}_i^T{}_c{}^t\mathbf{f}_i^{(k)} = 0 \tag{B.30}$$

where

$$\mathbf{H}_{ij}^{(k)} = \int_{\hat{\Gamma}_k} \hat{\mathbf{G}}_i^{(k)^T}\mathbf{Z}_u^{(k)^T}\hat{\mathbf{n}}^{(k)}\mathbf{Z}_\sigma^{(k)}\hat{\mathbf{F}}_j^{(k)}\,\mathrm{d}\Gamma \tag{B.31}$$

and

$${}_c{}^t\mathbf{f}_i^{(k)} = \int_{\hat{\Gamma}_k} \hat{\mathbf{G}}_i^{(k)^T}\mathbf{Z}_u^{(k)^T}\hat{\mathbf{n}}^{(k)}\mathbf{Z}_\sigma^{(k)}\mathbf{F}_c^{(k)}\,\mathrm{d}\Gamma \tag{B.32}$$

Note that the matrix $\mathbf{H}_{ij}^{(k)}$ is symmetric, and its definition is the same as that given in Eq. (90).

The first variation of the total potential can be cast as

$$\delta\pi = \sum_{k=1}^{K} \delta {}^{t}\hat{\boldsymbol{\alpha}}^{T} \mathbf{H}^{(k)} {}^{t}\hat{\boldsymbol{\alpha}} + \sum_{k=1}^{K} \delta {}^{t}\hat{\boldsymbol{\alpha}}^{T} {}_{c}{}^{t}\mathbf{f}^{(k)} = 0 \tag{B.33}$$

in which

$${}^{t}\hat{\boldsymbol{\alpha}}^{T} = \left\{ {}^{t}\hat{\boldsymbol{\alpha}}_{0}^{T}, {}^{t}\hat{\boldsymbol{\alpha}}_{1}^{T}, {}^{t}\hat{\boldsymbol{\alpha}}_{2}^{T}, \ldots, {}^{t}\hat{\boldsymbol{\alpha}}_{N}^{T} \right\} \tag{B.34}$$

and

$$\mathbf{H}^{(k)} = \begin{bmatrix} \mathbf{H}_{00}^{(k)} & \mathbf{H}_{01}^{(k)} & \cdots & \mathbf{H}_{0N}^{(k)} \\ \mathbf{H}_{10}^{(k)} & \mathbf{H}_{11}^{(k)} & \cdots & \mathbf{H}_{1N}^{(k)} \\ \vdots & \vdots & & \vdots \\ \mathbf{H}_{N0}^{(k)} & \mathbf{H}_{N1}^{(k)} & \cdots & \mathbf{H}_{NN}^{(k)} \end{bmatrix} \tag{B.35}$$

and

$${}_{c}{}^{t}\mathbf{f}^{(k)^{T}} = \left\{ {}_{c}{}^{t}\mathbf{f}_{0}^{(k)^{T}}, {}_{c}{}^{t}\mathbf{f}_{1}^{(k)^{T}}, {}_{c}{}^{t}\mathbf{f}_{2}^{(k)^{T}}, \ldots, {}_{c}{}^{t}\mathbf{f}_{N}^{(k)^{T}} \right\} \tag{B.36}$$

Defining

$$\mathbf{H} = \sum_{k=1}^{K} \mathbf{H}^{(k)} \quad \text{and} \quad {}_{c}{}^{t}\mathbf{f} = \sum_{k=1}^{K} {}_{c}{}^{t}\mathbf{f}^{(k)} \tag{B.37}$$

permits the expression for the first variation of the potential energy in its final form as

$$\delta\pi = \delta {}^{t}\hat{\boldsymbol{\alpha}}^{T} \mathbf{H} {}^{t}\hat{\boldsymbol{\alpha}} + \delta {}^{t}\hat{\boldsymbol{\alpha}}^{T} {}_{c}{}^{t}\mathbf{f} = 0 \tag{B.38}$$

This expression leads to the matrix equilibrium equation as

$$\mathbf{H} {}^{t}\hat{\boldsymbol{\alpha}} = {}_{c}{}^{t}\mathbf{f} \tag{B.39}$$

in which the unknown vector ${}^{t}\hat{\boldsymbol{\alpha}}$ represents the generalized coordinates associated with thermal deformations. The solution to this vector is obtained as

$${}^{t}\hat{\boldsymbol{\alpha}} = \mathbf{H}^{-1} {}_{c}{}^{t}\mathbf{f} \tag{B.40}$$

This solution permits the determination of the stress and displacement fields arising from thermal loading under zero boundary traction. Therefore, the expressions for ${}^{t}\boldsymbol{\sigma}_{p}^{(k)}$ and ${}^{t}\mathbf{u}_{p}^{(k)}$ are invoked as known quantities in the derivation of the global element stiffness matrix.

References

Akisanya, A.R., Fleck, N.A., 1997. Interfacial cracking from the free-edge of a long bi-material strip. International Journal of Solids and Structures 34, 1645–1665.

Bogy, D.B., 1968. Edge-bonded dissimilar orthogonal elastic wedges under normal and shear loading. ASME Journal of Applied Mechanics 35, 460–473.

Bradford, L.G., Dong, S.B., Nicol, D.A.C., Westmann, R.A., 1984. A central crack element in fracture mechanics. International Journal of Fracture 24, 197–207.

Chen, E.P., 1985. Finite element analysis of a bi-material interface crack. Theoretical and Applied Fracture Mechanics 3, 257–262.

Hein, V.L., Erdogan, F., 1971. Stress singularities in a two-dimensional wedge. International Journal of Fracture 7, 317–330.

Gadi, K.S., Joseph, P.F., Kaya, A.C., 1995. Enriched finite elements for a crack tip touching an interface. In: Proceedings of the ASME Materials Division, vol.-I, MD-Vol. 69-1. IMEC&E, Los Angeles, pp. 257–263.

Gadi, K.S., Joseph, P.F., Zhang, N., Kaya, A.C., 2000. Thermally induced logarithmic stress singularities in a composite wedge and other anomalies. Engineering Fracture Mechanics 65, 257–263.

Inoue, T., Koguchi, H., 1997. Relaxation of thermal stresses in dissimilar materials (approach based on stress intensity). International Journal of Solids and Structures 34, 3215–3233.

Lin, K.N., Mar, J.W., 1976. Finite element analysis of stress intensity factors for cracks at a bi-material interface. International Journal of Fracture 12, 521–531.

Madenci, E., Shkarayev, S., Sergeev, B., 1998. Thermomechanical stresses for a triple junction of dissimilar materials: global-local finite element analysis. Theoretical and Applied Fracture Mechanics 30, 103–117.

Mote, C.D., 1971. Global-local finite element. International Journal of Numerical Methods in Engineering 3, 565–574.

Munz, D., Yang, Y., 1992. Stress singularities at the interface in bonded dissimilar materials under mechanical and thermal loading. ASME Journal of Applied Mechanics 35, 460–473.

Munz, D., Yang, Y.Y., 1993. Stress near the edge of bonded dissimilar materials described by two stress intensity factors. International Journal of Fracture 60, 169–177.

Munz, D., Fett, T., Yang, Y.Y., 1993. The regular stress term in bonded dissimilar materials after a change in temperature. Engineering Fracture Mechanics 44, 185–194.

Pageau, S.S., Biggers Jr., S.B., 1996. Enriched finite elements for regions with multiple interacting singular fields. AIAA Journal 34, 1927–1933.

Pageau, S.S., Biggers Jr., S.B., 1997. Enrichment of finite elements with numerical solutions for singular stress fields. International Journal of Numerical Methods in Engineering 40, 2693–2713.

Qian, Z.Q., Akisanya, A.R., 1999. Wedge corner stress behavior of bonded dissimilar materials. Theoretical and Applied Fracture Mechanics 32, 209–222.

Rice, J.R., Sih, G.C., 1965. Plane problems of cracks in dissimilar media. ASME Journal of Applied Mechanics 32, 418–423.

Theocaris, P.S., 1974. The order of singularity at a multi-wedge corner of a composite plate. International Journal of Engineering Science 12, 107–120.

Williams, M.L., 1952. Stress singularities resulting from various boundary conditions in angular corners of plates in extension. ASME Journal of Applied Mechanics 19, 526–528.

Yuuki, R., Cho, S.-B., 1989. Efficient boundary element analysis of stress intensity factors for interface cracks in dissimilar materials. Engineering Fracture Mechanics 34, 179–188.